A Morphological Investigation of Submarine Volcanic Cones and their Relation to Crustal Stress, Adare Basin, Antarctica

Senior Thesis

Submitted in partial fulfillment of the requirements for the

Bachelor of Science Degree

At

The Ohio State University

By

Daniel J. Barr

The Ohio State University

2014

Approved By

Terry J. Wilson, Advisor

The Ohio State University

Abstract

Numerous methods to determine the state of stress in the Earth's crust have been developed, including mapping geologic faults and measurements in boreholes. Recently, a new method has been brought forth that uses a common and distinctive feature on the Earth's surface: volcanoes, specifically, monogenetic volcanoes formed in a single eruption. This research project describes how the shape and alignment of volcanic cones can be used to determine the state of stress in the crust in a region of Antarctica known as the Adare Basin. Numerous submarine volcanic cones formed in association with rifting events that stretched the crust in the Ross Sea area. Mapping of the seafloor by bathymetric sonar attached to the hull of the research vessel *RVIB Nathaniel B. Palmer* revealed the volcanoes and provided digital elevation data. For this project, the digital bathymetric data were used for morphologic analysis. Hillshade and slope maps, together with slope profiles, were used to identify the change in slope defining the exact base of the volcanic cones and their size and shape. The seafloor volcanoes vary in diameter, and are characterized by sharp, conical summits. The slopes of 47 randomly selected cones were analyzed to produce an average value for the break in slope of the base of each cone, from which a custom color ramp in ArcGIS was created to identify the base of the cones, and their shape. Circles or ellipses were drawn from the center of these cones to document elongations and the ratio of their axes. Alignments were then drawn along linear cone arrays and assessed to determine their reliability, based on the shape of the cone, number of cones in the alignment, distance from a best-fit line by orthogonal regression, and the distance between each cone. There were two sets of alignments found, one with a N-S trend and another with an E-W trend, and both sets of alignments received low grades from the assessment criteria. The N-S trending alignments share a common orientation with rift structures and normal faults that occur further out in the Adare Basin, while the E-W trending alignments likely were formed by a change in the state of stress in the crust related to the pressure and heating from the upwelling magma in the region.

Acknowledgements

I would first like to thank my advisor, Dr. Terry Wilson, for allowing me the opportunity to study such an interesting topic and giving me sound advice along the way, both in terms of geology and life in general, and having the patience to deal with my sometimes less-than-optimal availability to work on this project.

Jie Chen deserves many thanks, for his help in understanding Linux and the Fledermaus software that was used in this research project. Without his help, I would have gotten nowhere, and would likely still be staring at a computer screen with a confused look upon my face.

Stephanie Konfal also deserves recognition, for her help in teaching me the finer points of ArcGIS and Excel, as well as other valuable insights and advice on research techniques.

My parents also deserve acknowledgement, as they have had to put up with my constant lack of communication and inability to visit home while working on this project, and I appreciate their constant loving support of me and my endeavors and dreams.

I wish to give my thanks to the entirety of the School of Earth Sciences. The faculty, staff, and my fellow students have allowed me to gain the knowledge and abilities to complete this project successfully in a fun environment, and for that I'm thankful.

Finally, the data that was used in this research project was from the Antarctic and Southern Ocean Portal (http://www.marine-geo.org/portals/antarctic/). These data were made available through the Marine Geoscience Data System (MGDS) and the corresponding GeoMapApp 3.3.0, which is hosted by the Lamont-Doherty Earth Observatory at Columbia University. I would like to thank NSF for funding the Antarctic and Southern Ocean Portal and MGDS, and Columbia University for hosting the latter.

Table of Contents

Introduction

The state of stress in the crust is an important aspect of earth science, as it has a profound effect on most geological processes. The search for new ways to measure and determine stress is a constant endeavor within the field of Earth science. The most common methods for determining crustal stress come from seismic measurements from earthquake activity and from measurements in boreholes. For Antarctica, little seismic data have been recorded due to anomalously low seismic activity, and drilling efforts have been rare due to the extreme amounts of coordination and resources to achieve them. Therefore, alternate methods of determining stress in Antarctica are needed.

Unique tectonic and geologic events have shaped the Antarctic continent over the past 160 million years, since the breakup of Gondwanaland in the late Jurassic, and eventual formation of Antarctica, Africa, and Australia [Fitzgerald, 2002]. New methods to record and measure these past events are an important part of the exploration of Antarctica as are understanding the stress regimes associated with the rift history of Antarctica during its break up from Gondwanaland.

This study focuses on the analysis of alignment and shapes of volcanic cones on the seafloor in the Adare Basin to obtain new information on the regional stress of the West Antarctic Rift System (WARS) in the northwestern Ross Sea, Antarctica.

Geologic History

The Adare Basin and the adjoining Ross Sea are considered to be a part of a region of Antarctica known as the West Antarctic Rift System (WARS), one of the largest rift systems on Earth, comparable in size to the Basin and Range region of Western North America, and the East

African Rift [Behrendt, 1999]. The WARS is composed of a series of rift basins, with the youngest rifting located in the western Ross Sea [Fitzgerald, 2002].

A rift basin is a geologic setting in which the crust experiences tensional forces that result in the crust thinning as it is pulled apart, due to displacements on normal fault systems (Figure 1). This allows warm magma underneath the crust to well-up and create fractures, the feeder dikes for surface volcanism that also produce extension of the crust.

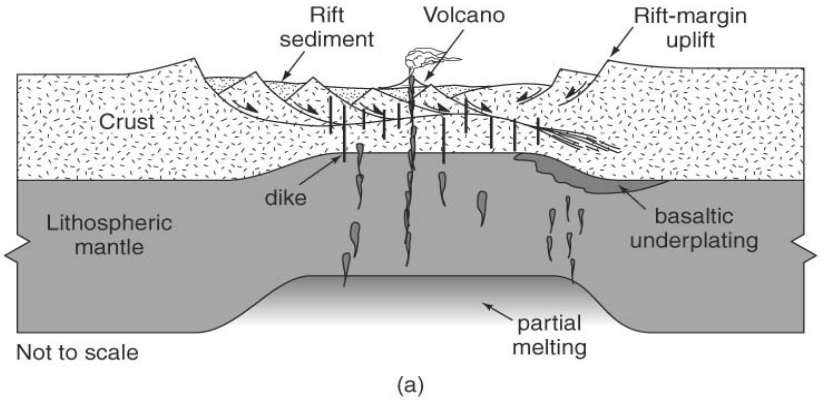

Figure 1: Diagram Profile View of an Active Rift Zone [Van der Pluijm, 2004]

Rifting in the WARS is dated to the early Cretaceous, and has continued in periodic events through the Cenozoic [Behrendt, 1999]. Some of the basins present in the Ross Sea area are former rift structures that began forming during the breakup of Gondwanaland in the late Jurassic [Fitzgerald, 2002]. The structure of the WARS is an asymmetric rift system, with one flank being uplifted over the past 60 million years by buoyant mantle underneath, with uplift rates as much as 1 km/m.y at times throughout its history, creating the Transantarctic Mountains [Behrendt et. al, 1991]. Total extension in the WARS is difficult to calculate, with values ranging from 400 km to upwards of 1800 km [Fitzgerald, 2002].

The Adare Basin itself was part of a spreading center in the crust in the westernmost part of the WARS [Cande et al., 2000; Granot et al., 2010]. Magnetic anomalies from the seafloor have dated the spreading to have occured from 43-26 Ma, or Eocene to Oligocene [Granot, 2013; Cande and Kent, 2006: Cande et al., 2000] In this time period, the amount of separation between East and West Antarctica is estimated to be near 180 km [Cande et al., 2000]. Figure 2 shows a map of the Adare Basin and rift structures in the WARS, with the inset box highlighting the area of study.

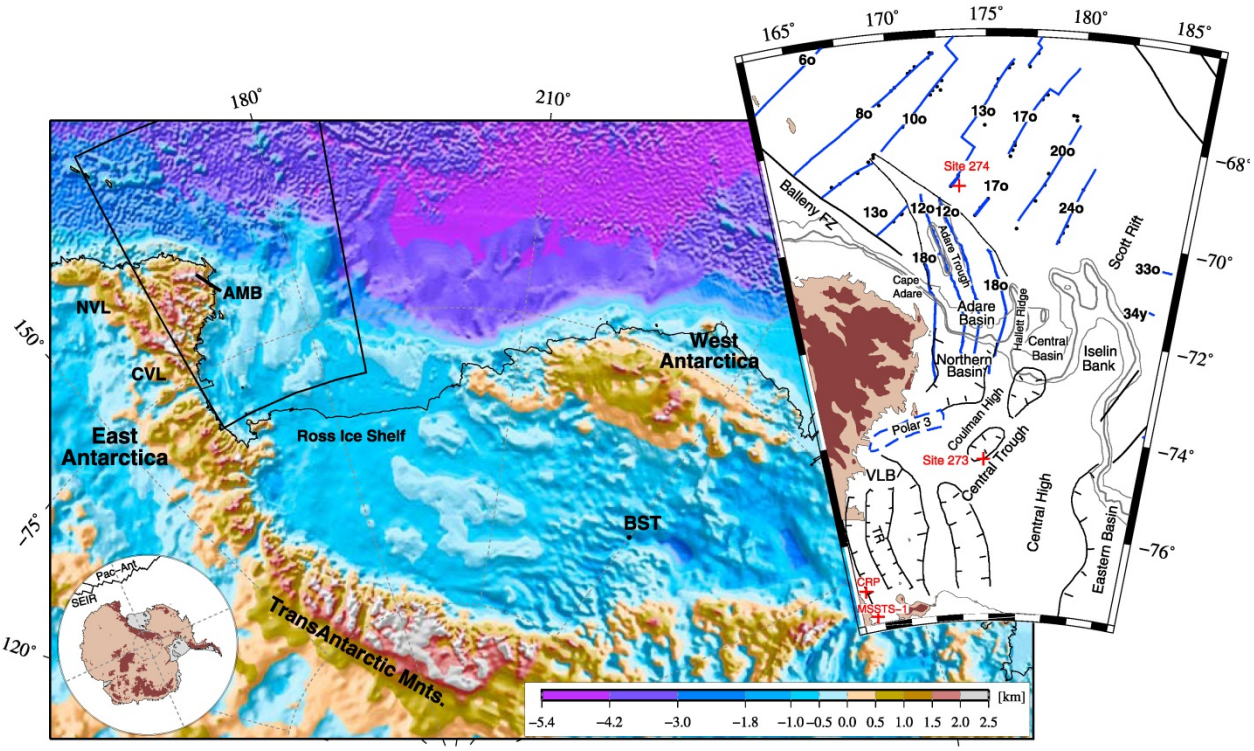

Figure 2: Map of West Antarctica, with inset map highlighting the Ross Sea, and Adare Basin field of study outlined by the black box in the inset map [Granot et al. 2010].

Granot et al. (2010) document another pulse of rifting activity that occurs in the Miocene around 17 Ma, based on seismic reflection profile analysis and comparing the ages of the sediments overlaying the tilted faults blocks underneath. The tilted blocks resulting from this

Miocene rifting event show a normal fault trend of NE-SW with the normal faults displaying an *en echelon* pattern, shown in Figure 2 [Granot et al., 2010].

Geochemical analysis from dredged rocks in the Adare Basin show an intriguing similarity to rocks from the WARS further inland, giving more evidence to support the claim that the rifting events in the Adare Basin are linked to those occurring in the WARS [Granot et al., 2010].

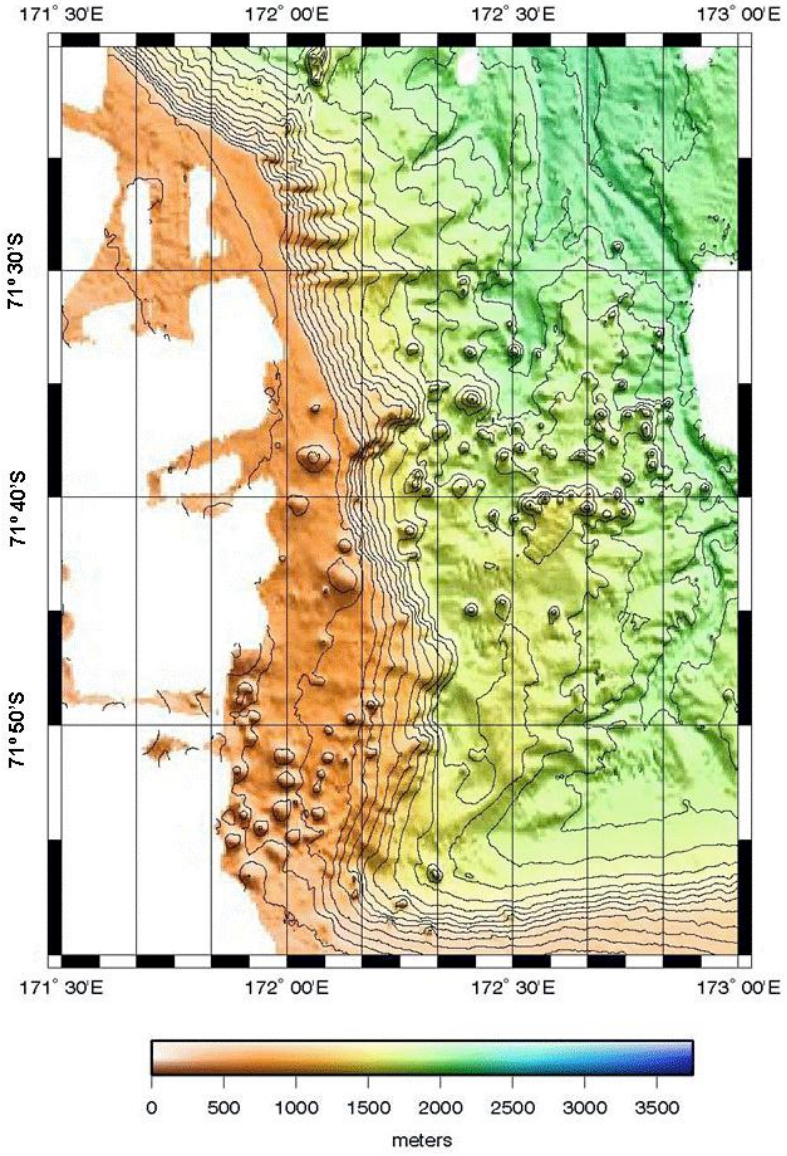

Figure 3: Bathymetric image of the southern Adare Basin seafloor, with the field of volcanic cones in the area of study outlined by the black box [Granot et al. 2010].

Widespread volcanism is associated with rifting in the Adare Basin, including rocks of the McMurdo Volcanic Group, exposed on land, and consisting of a series of alkaline volcanic rocks. The McMurdo Volcanic Group is divided into several distinct subgroups, including the Hallett, Erebus, and Melbourne Provinces [Kyle, 1990]. The Adare Basin volcanics are located offshore of the Hallett Volcanic Province, and have similar geochemical signatures to the McMurdo Volcanic Group [Panter and Castillo, 2007].

Methods

I. Stress Determined from Volcanic Alignments

During volcanic eruptions, magma moving upwards through the crust creates opening-mode fractures by hydraulic pressure of the surrounding host rock, in order to allow magma to reach the surface. Features such as radial dike swarms and flank volcanoes are evidence of such stresses acting on the surrounding rock near volcanic vents [Nakamura, 1977]. These features form perpendicular to the least principal stress plane in the crust, and parallel to the maximum principal stress plane [Anderson, 1951]. In monogenetic volcanic cones, a single volcanic event has occurred to create the features seen on the surface, recording the state of stress in the crust at that point in time. If multiple monogenetic volcanic features (cones, dikes, fissures, etc.) show a preferred alignment on the surface (rows or series of linear features that share a similar trend) in both trend of cones and elongation of cone shape, and are of a similar age, then it is possible the alignment of those surface features is due to an underground feeder dike preferentially aligned with the stress regime that existed at that time [Nakamura, 1977]. By identifying a pattern in the elongation and trend of the volcanic cones, an alignment can be identified and mapped. If

multiple alignments with the same trend are present, their orientations define the stress directions at the time the cone arrays were formed.

II. Bathymetric Data Collection and Processing in Fledermaus

Bathymetry refers to the topography that exists on the seafloor. To measure bathymetry accurately, ships are equipped with multibeam sonar echosounders that emit sound waves and then listen for them to bounce off the seafloor. Multibeam refers to the numerous echosounders and transmitters mounted on a single ship, increasing the coverage of the seafloor. The instrument measures the amount of time it took for the sound to bounce back, which is controlled by the distance from the echosounder to the seafloor (depth) plus other factors such as water salinity and temperature. These measurements are then recorded to create an image of the seafloor. Other variables such as the pitch of the ship on the surface of the ocean are also factored into the calculations.

The data used in this thesis were obtained by the RVIB *Nathaniel B. Palmer* off the coast of northern Victoria Land in the northwestern Ross Sea. All *Palmer* data are archived and made available through the Southern and Antarctic Ocean Portal (SAOP), part of the Marine Geosciences Data Systems (MGDS) housed at the Lamont-Doherty Observatory at Columbia University [http://www.marine-geo.org/portals/antarctic/]. The SAOP contains data including "seafloor bathymetry, subbottom profiling, trackline gravity and magnetics, meteorological, and water column data as well as basic cruise information for the Palmer and Gould expeditions" [http://www.marine-geo.org/portals/antarctic/]. MGDS's GeoMapApp 3.3.0 was used to find the tracks of the RVIB *Nathaniel B. Palmer* that covered the study area, and these data were downloaded in MBSystems format, created and maintained by the Monterey Bay Aquarium

Research Institute and the Lamont-Doherty Observatory as “an open-source software package for the processing and display of bathymetry and backscatter imagery data derived from multibeam, interferometry, and sidescan sonars” [http://www.mbari.org/data/mbsystem/html/mbsystem_home.html]. These data were transferred to a computer with a Linux-based operating system in order to convert the MBSystems files into ASCII (xyz) format. The converted data were then uploaded into QPS’s *Fledermaus*™ software for editing and processing. *Fledermaus*™ is an interactive 4D geo-spatial processing and analytical tool [http://www.qps.nl/display/main/home/] that allows the user to view the data from a 3D point of view, as well as correct the data for inconsistencies and errors that originated from the initial data collection. Figures 4-6 show 3D profile views of the area of study in *Fledermaus*™.

The first phase of data processing involved removing data that were of no concern to the current study. Areas that contained no visible cones or extended well beyond the field of study were removed, and any data that appeared to disagree with its surrounding data points (erroneous data points, gaps in the coverage, etc.) were also removed. By the end of this stage of processing, the area of the study had been defined and condensed to a smaller region.

The second stage of processing involved the cleaning of the data. Several areas of the data showed sign of “railroad” artifacts, appearing as a series of parallel lines that look like railroad ties, created along the path of the research vessel recording the multibeam sonar. Also, erroneous data points gave rise to impossible seafloor features such as spikes and pits mere feet wide, but anywhere from ten to hundreds of feet tall. Both the railroad artifacts and erroneous data points were removed by deleting the data points responsible for the artifacts before moving on.

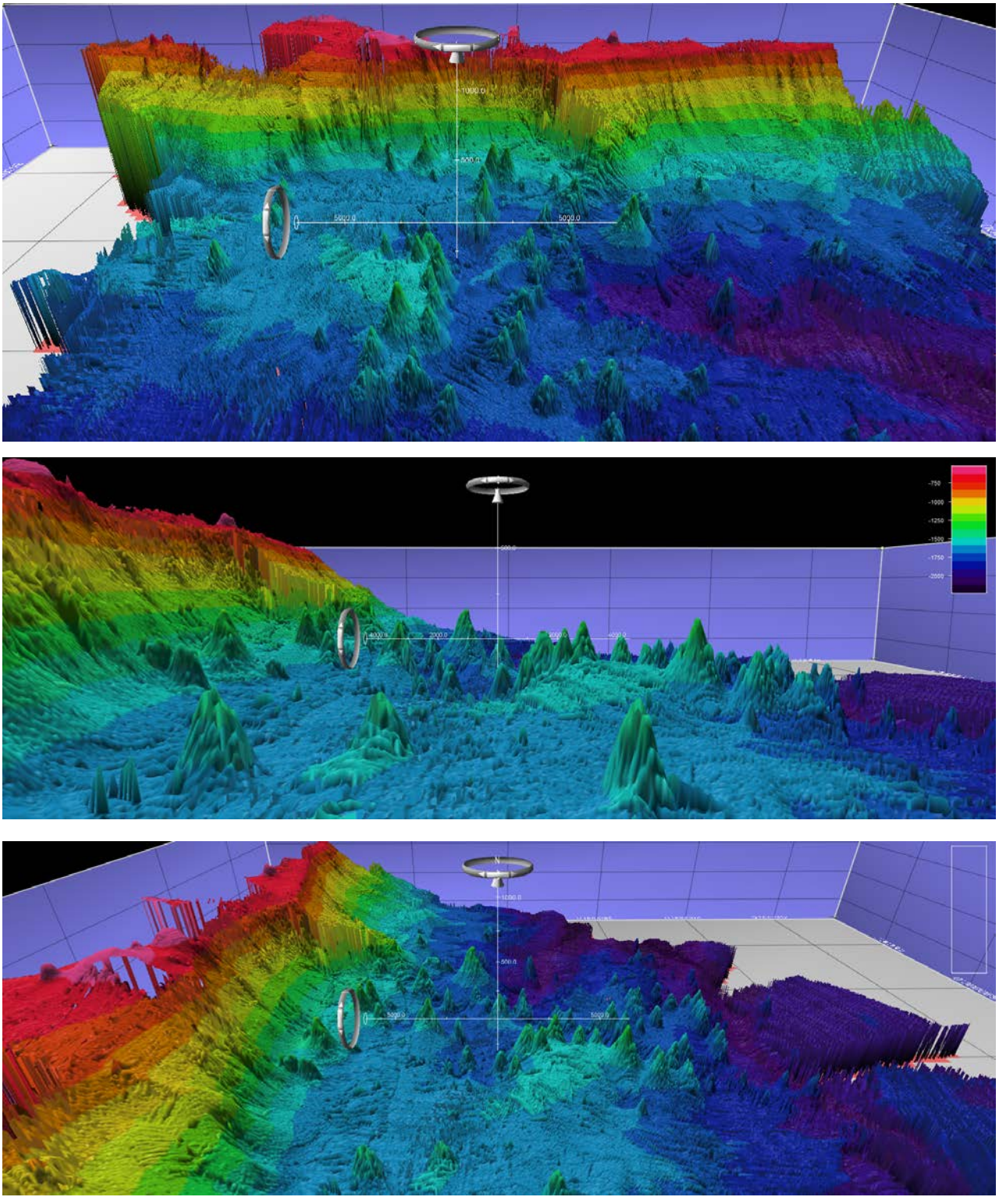

Figures 4-6: Various 3D profile views of the Adare Basin study region taken in *Fledermaus*™, with the red arrows indicating north.

The final step in the processing of the bathymetric data was to fit the correct bin or grid size to the data to create a continuous bathymetric map. When a ship is collecting sonar measurements while moving, the recording equipment sometimes creates gaps in the bathymetric data where the ship simply moved ahead and missed the returning sonar waves, or the pitch of the waves causes the ship to incorrectly gather sonar waves to the wrong sensors. These gaps increased in frequency and size as the speed of the ship taking the measurements increased. This was corrected in Fledermaus by creating a larger bin size, a grid point spacing in meters that allowed the surrounding data to compensate for the missing data in the interpolation process. In this study, a bin size of 50 meters was found to be the best fit to retain the quality of the data, while at the same time not degrading the quality of the surrounding data, since increasing the bin size too much can cause the surrounding data to be stretched and exaggerated.

III. Data Analysis of Cone Slope

After the bathymetric data were finalized, the data were transferred into ArcGIS 10.1 and slope and hillshade maps were generated to identify the shape and degree of slope of the cone flanks. To quantify accurately the profile of the cone, the slope of the cones sides, the apron (break in slope) near the base of the cone, and the slope of the seafloor were all measured. To accomplish this, each cone was assigned a number and a 2D cross-section profile was created in ArcGIS to identify where the ‘break in slope’ from the apron to the seafloor occurred. This provided an accurate method to determine where the actual base of the cone begins in comparison with the seafloor. A total of 47 volcanic cones were analyzed to determine the average slope values for the cone flanks, the cone apron, and the adjacent seafloor, in order to

define the base of the volcanic cones. Figure 7 shows a map of each of the cones and the number they were assigned.

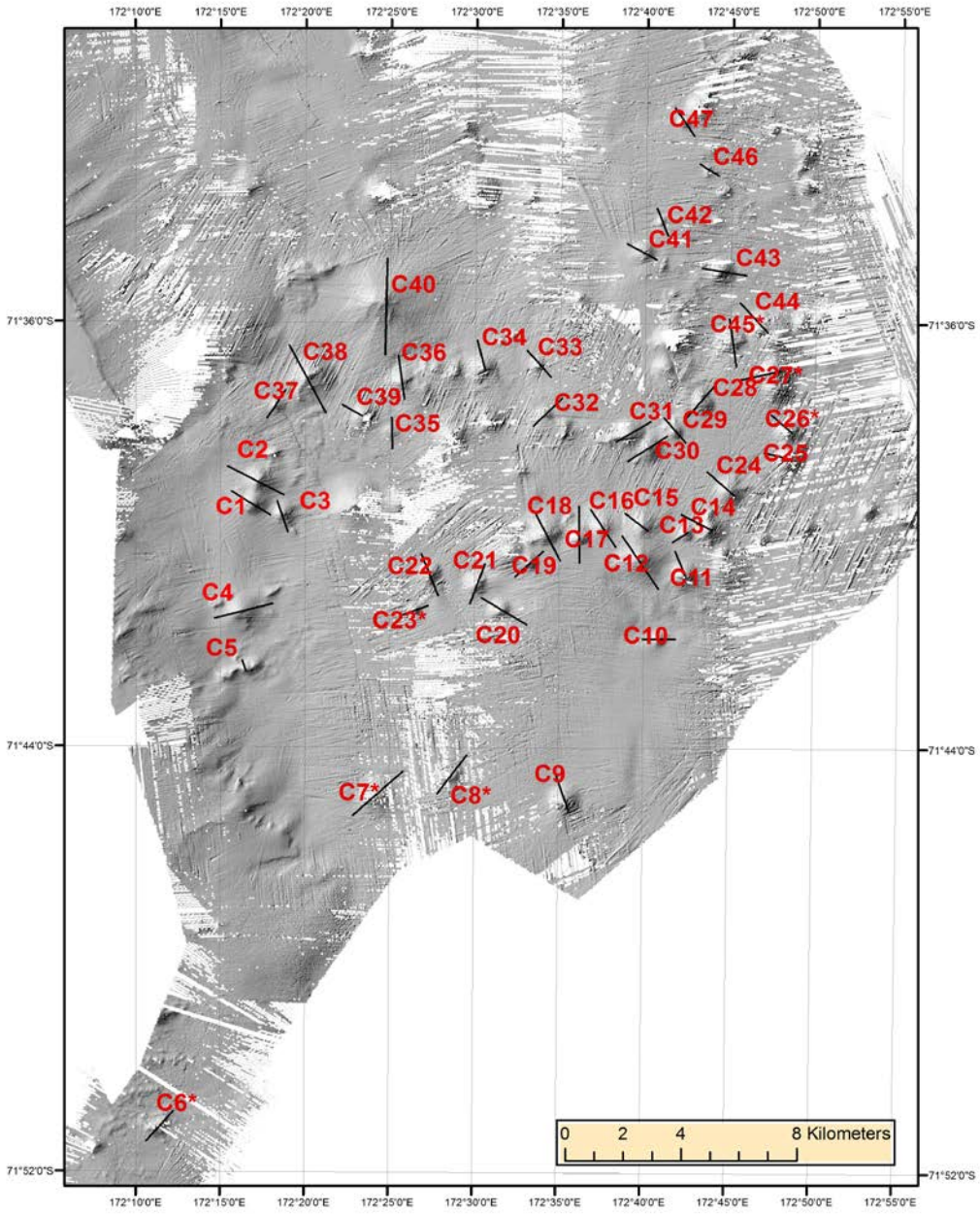

Figure 7: Hillshade map with Cone ID Number and line of profile marked

Cone profile data were exported to Microsoft Excel, where the data were graphed using a scatter plot with smooth lines, with distance in meters on the x axis and elevation in meters on the y axis. Linear trendlines were fit to the profile data to identify the average slope of the seafloor, the average slope of the apron of the cone, and the average slope of each side of the cone. This resulted in as many as 5-6 trendlines created for each cone profile. Figures 8-10 are representative profiles taken of cones in the Adare Basin region. Due to some of the data being incomplete and containing gaps that *Fledermaus*™ was unable to correct for, some cone profiles consisted of only one flank of the cone, in order to minimize error in the data set.

Figures 8A-C: Three cone profiles, with the equations of slope for each section of the cones marked and color coded and trendlines in place. Cone #11 is an example of a partial profile.

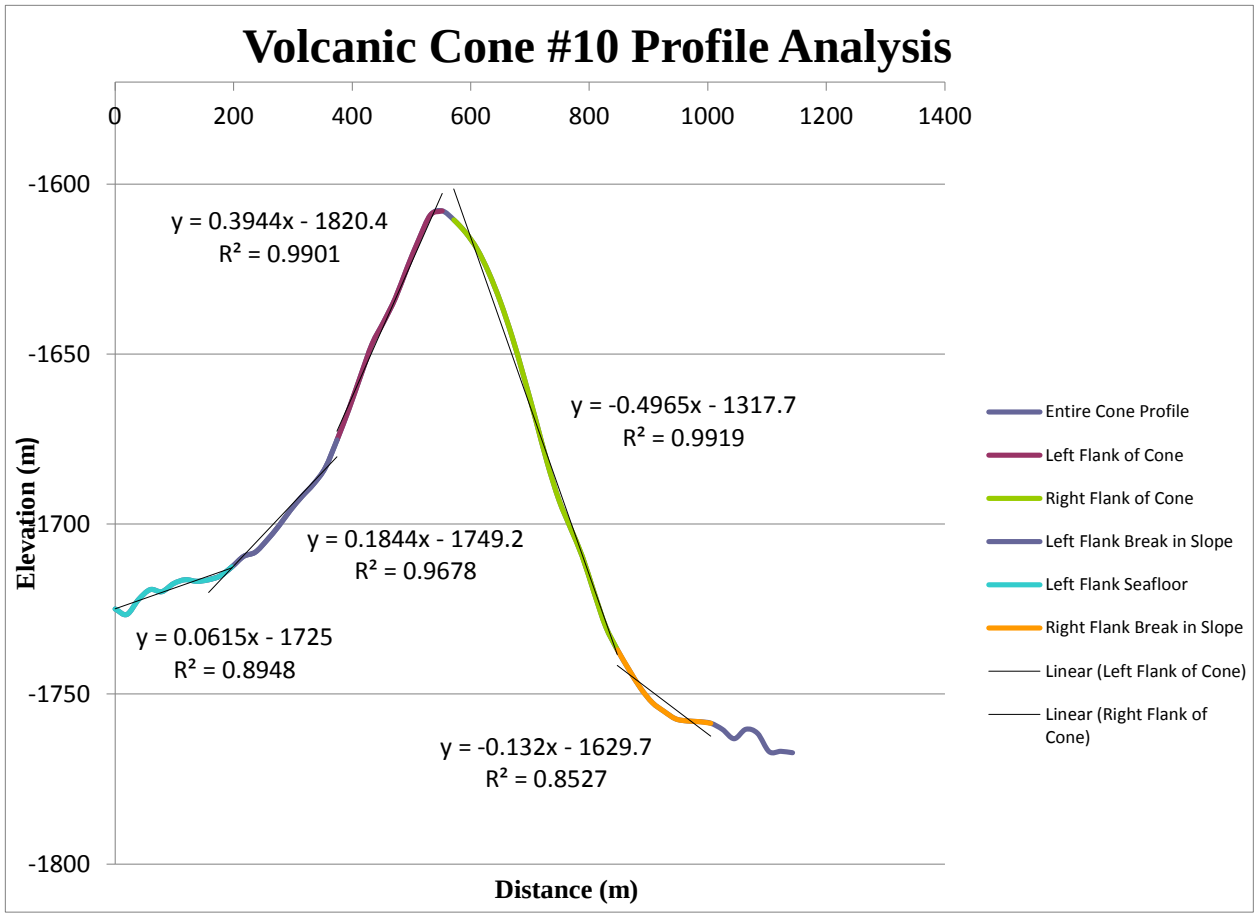

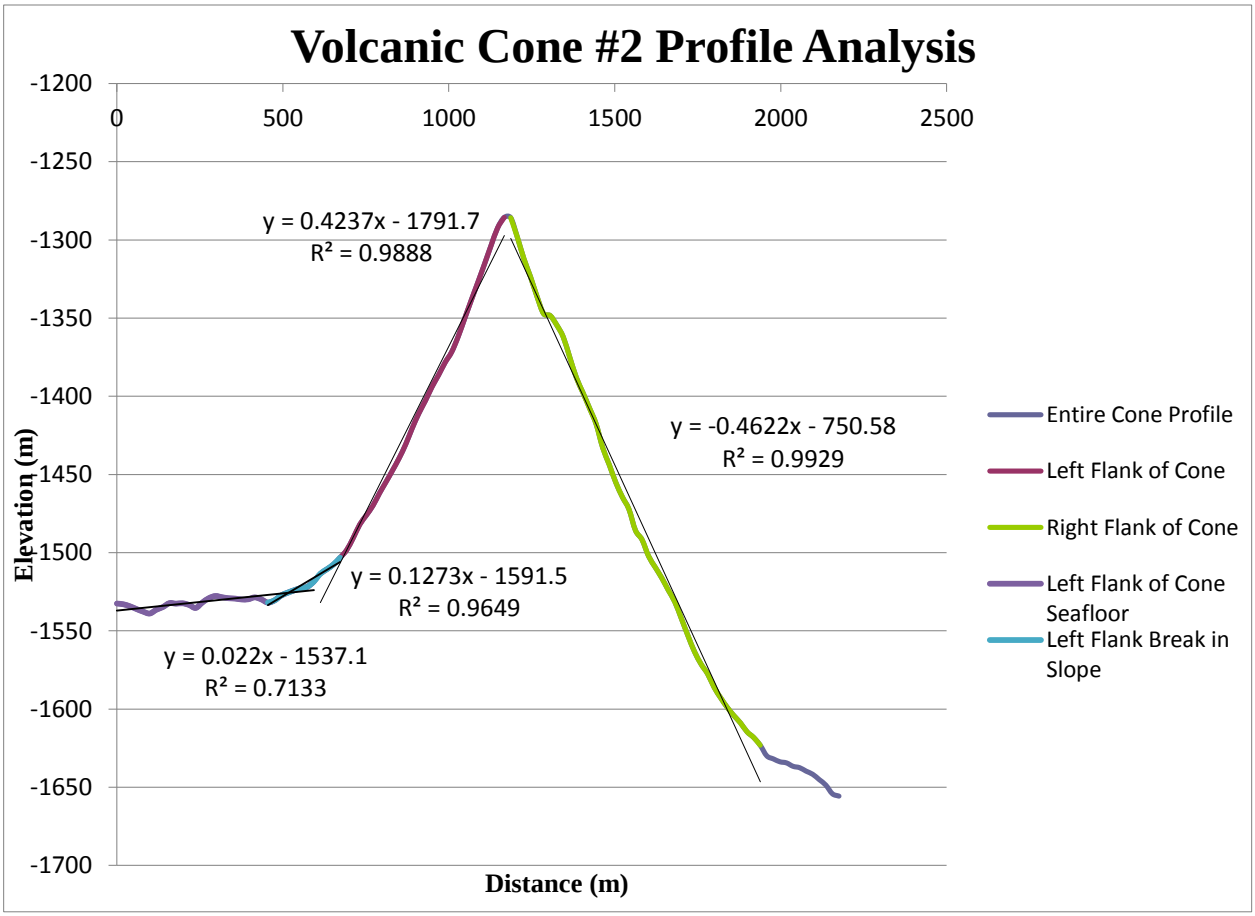
Volcanic Cone #2 Profile Analysis
-1200
-1250
-1300
-1350
-1400
-1450
-1500
-1550
-1600
-1650
-1700
0
500
1000
1500
2000
2500
Elevation (m)
Distance (m)
y = 0.4237x - 1791.7
R² = 0.9888
y = -0.4622x - 750.58
R² = 0.9929
y = 0.1273x - 1591.5
R² = 0.9649
y = 0.022x - 1537.1
R² = 0.7133
Entire Cone Profile
Left Flank of Cone
Right Flank of Cone
Left Flank of Cone Seafloor
Left Flank Break in Slope

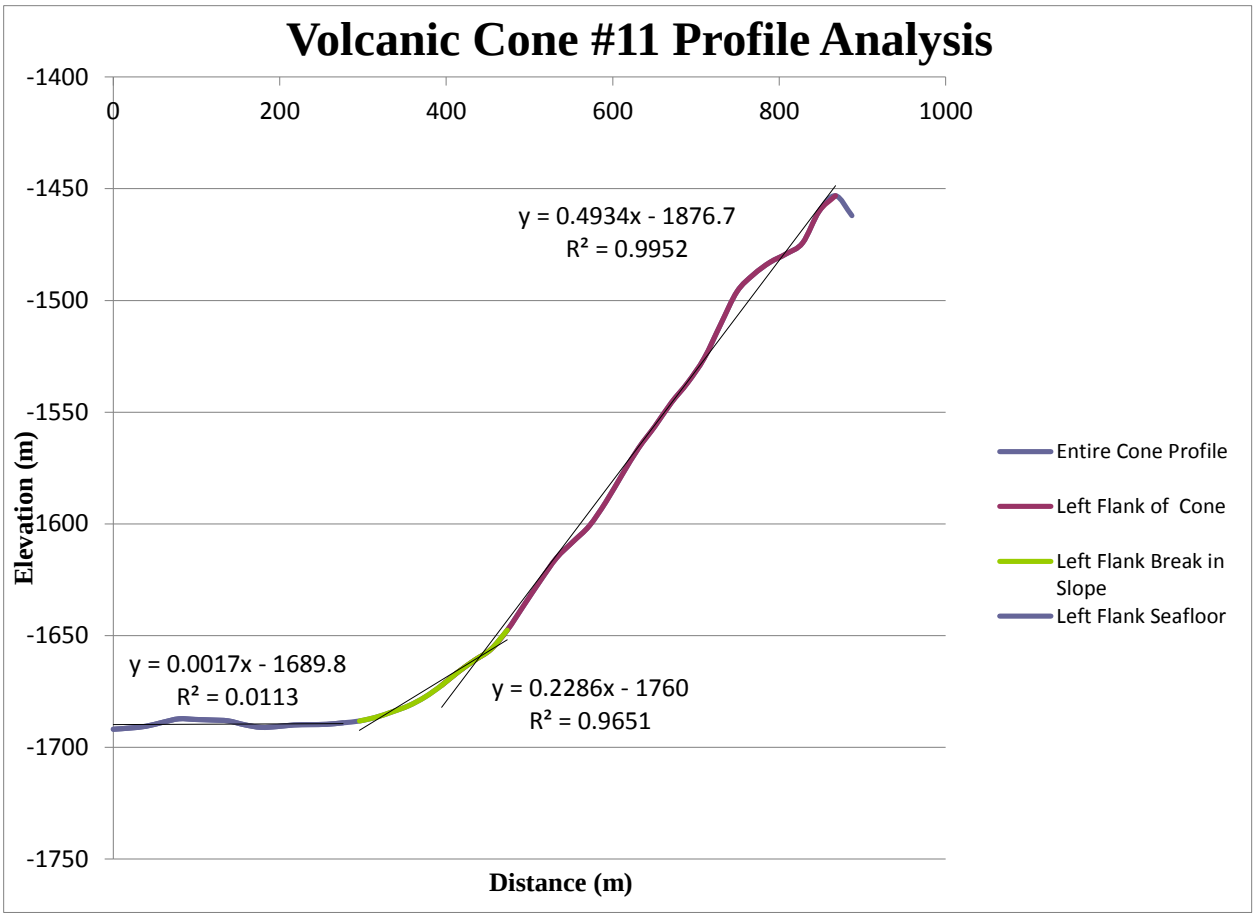
Volcanic Cone #11 Profile Analysis
-1400
-1450
-1500
-1550
-1600
-1650
-1700
-1750
0
200
400
600
800
1000
Elevation (m)
Distance (m)
y = 0.4934x - 1876.7
R² = 0.9952
y = 0.0017x - 1689.8
R² = 0.0113
y = 0.2286x - 1760
R² = 0.9651
Entire Cone Profile
Left Flank of Cone
Left Flank Break in Slope
Left Flank Seafloor

The values of the slope for the linear trendlines for each sector of the cones were averaged and converted into degrees. The overall average value of the slope angle of the flanks of the cones averaged 38-41 degrees, the slope of the cone aprons averaged 13-17 degrees, and values for the slope of the seafloor averaged 2-3 degrees. Figure 9 shows a table of the values calculated from the cone slope analysis.

Criteria	Left Seafloor	Left Apron	Left Flank	Right Flank	Right Apron	Right Seafloor
Average Rise/Run	0.020371429	0.173736842	0.43718085	0.40244	0.139461905	0.025
Average Degree	2.036861102	17.20096403	41.13049333	38.2034783	13.85647236	2.499479297
Average Degree Rounded	2.03°	17.2°	41.0°	38.0°	13.9°	2.50
Standard Deviation	0.021283696	0.049264632	0.08156921	0.088973956	0.048208179	0.005556078
90% Confidence Interval, Rise/Run	0.015767183	0.015663886	0.02332026	0.029477113	0.020618979	0.006287294
90% Confidence Interval, Degree	1.576587616	1.566260527	2.33160339	2.946857862	2.061605726	0.628721101
90% Confidence Int. Rounded	1.57°	1.56°	2.33°	2.94°	2.06°	0.62°
Final Results	2.03° ± 1.57°	17.2°±1.56°	41.0° ±2.33°	38.0° ±2.94°	13.9° ±2.06°	2.50° ±0.62°

Figure 9: Table of Data from Cone Analysis with Final Slope Values Calculated

IV. Mapping of Cones and Determining Ellipsoidal Shape

With the established average values for the slopes of the cone aprons and the seafloor from the previous analysis, a custom color ramp was built in ArcGIS to highlight a visual

boundary between the slope of the seafloor and the flanks of the cone. Cooler colors such as blue and green represent shallow values of slope and warmer colors such as yellow and red represented the steeper values, with the green-to-yellow boundary marking the change between the seafloor and the apron of the cone. The green color range covered the values of 3 to 7 degrees of slope, while yellow colors covered the values from 7 to 12 degrees.

To ensure the slope angle analysis was in agreement with the custom color scheme, a sampling of cones from random locations across the region were used to compare where the Excel profiles had the break in slope compared to the ArcGIS color scheme. Tests of multiple cones showed that the location of the apron on the Excel profiles closely matched to the green-to-yellow boundary in the slope map created in ArcGIS. With this confirmed the base of each cone was then mapped by creating a shapefile in ArcGIS and using the polygon tool to map the green-yellow boundary. Due to some distortion in the data, however, some liberty was taken to prevent artifacts in the bathymetry data from distorting the true shape of the cone base, such as leftover railroad artifacts that created a discrepancy in the slope map, giving values of higher slope values where none existed.

Each cone was then fitted with either an ellipse or a circle. To do this, the centers of each cone were calculated using the add-in Easy Calculate 10 in ArcGIS. The X and Y values were calculated and entered into the attribute table of the cone base shapefile, and these coordinates were then exported into Excel. In Excel, the data were converted into a .csv file, and this file was imported back into ArcGIS to create a new shapefile of each cone's center point.

Each cone then had a circle or ellipse drawn outwards from this center point as a third shapefile using ArcGIS's polygon tool. The long and short axes of each ellipse for elongated

cones were drawn in two separate shapefiles to highlight the direction of elongation of the cones, which reveals the probable trend of the associated alignment. Each axis was drawn using bounding rectangles as a reference frame around the ellipses in order to accurately measure the length of each axis.

V. Alignment Selection and Reliability Assessment

The Paulsen and Wilson (2010) method for determining the quality and reliability of volcanic cone alignments was used in this study to assess the alignments made for the NAVF (Northern Adare Volcanic Field). The assessment system used is based on a graded system (A>B>C>D) in which four criteria are used to judge the quality of alignments: 1) the number of vents in each alignment, 2) the standard deviation of the vent centers from a best-fit line drawn using orthogonal regression, 3) evaluation of vent elongation (number of elongate vents, ratio of short and long axes, orientation of long axes relative to alignment trend), and 4) spacing of cones along alignment (Figure 10). Each grade reflects the confidence level that a particular alignment correlates to a plausible underground feeder dike system producing the volcanic cones (ex. an A alignment has a higher confidence level than a B alignment, etc.), to show the overall reliability of the alignments drawn for a particular region.

Reliability grade	# vents	Standard deviation best-fit line distance (m)	Index of vent elongation	Standard angular deviation vent long axes (°)	Average vent spacing distance (m)
A	≥4	≤125	1 cleft cone -or- 1 fissure ridge -or- 2≥1.6 -or- 1≥1.6 and 1≥1.4	≤30	No limit
	≥5	≤100	No shape data	No shape data	≤600[a] or ≤800[b]
B	≥3	≤150	1≥1.6 -or- 2≥1.4 -or- 1≥1.5 and 2≥1.2	≤35	No limit
	≥4	≤125	No shape data	No shape data	≤600[a] or ≤800[b]
C	≥2	≤175	1≥1.4 -or- 2≥1.2	≤40	No limit
	≥3	≤150	No shape data	No shape data	≤800[a] or ≤1000[b]
D	≥2	>175	1≥1.2	>40	No limit
	≥3	>150	No shape data	No shape data	>800[a] or >1000[b]

Figure 10: Volcanic Cone Alignment Assessment Table [Paulsen & Wilson, 2010]

Alignments linking multiple vents were drawn using the polyline tool in ArcGIS based on the shape of the cones and whether they were clustered together along a linear trend. Multiple alignment sets were drawn, with each tested to assess reliability. The distance between the centers of each cone, the azimuth of the long axis of each elongate cone, the ratio of each elongate cone's long axis to short axis, and the azimuth of the alignment itself were measured.

The standard deviation of each cone to a best-fit line was determined through GraphPad Prism 6.0, a statistical analysis software package that was used to calculate the orthogonal distance of each cone center to a best-fit line, from which a standard deviation of the cones from the generated best-fit line could be calculated. All of these measurements were used in the final assessment of cone grades to determine how reliable each cone alignment was.

Results

The Paulsen and Wilson (2010) reliability table shows that the grades for the alignments chosen in this study were on the low end of the assessment scale, with most alignments receiving a grade of C or lower, and with a few alignments meeting none of the requirements of being a grade D alignment. This shows that, while the surface features appear to have an alignment, the statistical analysis indicates that these are not reliable alignments, as defined by the method used for terrestrial scoria cones developed by Paulsen and Wilson (2010). Figure 11 shows the data from the alignment analysis and the grades each individual alignment received.

Alignment ID	Std. from Best Fit Line (m)	Alignment Azimuth (°)	Cone L.A. Azimuths (°)	Avg Dev. of Vent Long Axes (°)	# Cones in Alignment	LA:SA Ratios	Avg. Distance B/w Vents (m)	Alignment Grade
1	120	51	60	9	4	1.21	1634	C
2	72	87	64, 97	17	3	1.28, 1.37	1980	C
3	399	84	73, 76, 97	10	4	1.32, 1.57, 1.55	885	C
4	N/A	81	80, 87	3	2	1.47, 1.41	829	D
5	N/A	84	88, 81	3	2	1.26, 1.26	2268	C
6	691	90	N/A	N/A	3	N/A	3371	C
7	402	100	74	26	3	1.3	1433	C
8	346	86	77	9	7	1.33	987	C
9	149	55	47	8	4	1.37	1931	C
10	259	150	152, 108	22	5	1.26, 1.77	1762	C
11	130	74	56, 8	42	3	1.15, 1.31	1229	C
12	310	90	92, 100, 85	6	6	1.95, 1.32, 1.60	1836	C
13	120	88	75	13	5	1.26	1181	C
14	290	13	94, 156	59	3	1.54, 1.36	1507	C
15	N/A	156	N/A	N/A	2	N/A	2325	D
16	N/A	64	N/A	N/A	2	N/A	1302	D
17	N/A	10	49	39	2	1.45	1147	D
18	N/A	75	76	1	2	1.35	859	D
19	57	91	N/A	N/A	4	N/A	3180	C
20	N/A	82	70, 77	8	2	1.57, 1.28	1044	D
21	N/A	82	88, 81	3	2	1.27, 1.20	537	D

Figure 11: Table of measurements of standard deviation from calculated best fit line (in meters), azimuth of cone alignment (in degrees), the azimuth of elongate cones long axis (in degrees), the average deviation of elongate cones azimuth from the alignment's azimuth (in degrees), the overall number of cones in the alignments, the ratio of lengths of each elongate cones long axis to short axis, the average distance between each cone (in meters), and the final grade each alignment received.

With the hillshade and slope maps (Figures 12, 13, & 15), 93 cones were mapped in the northern Adare volcanic field, with 40 of them showing signs of elliptical shape that was easily identified. The remaining cones were mapped as circular cones, even if slightly elliptical, in order to prevent bias in identifying the orientation of the alignments. Most cones had a diameter that ranged between 900 and 1300 meters, with elongate cones having long axes that reached more than 2000 m. Also, some smaller cones did occur with diameters < 500m. Over 70% of the cones on the seafloor have heights that fall within the range of 150m to 250m, with all of them displaying a sharp conical point with no crater at the summit. A handful of cones had heights below 150 m or above 250m.

The slope of the cones varied depending on the region of the cone measured, with the flank of the cone averaging between 38 and 41 degrees, and the apron at the base of the cone averaging 13-17 degrees. Figure 13 depicts slope using a gradient scale, rather than slope angle in degrees. Gradient is rise over run, with a 0 degree slope having a gradient of 0, a 45 degree surface having a gradient of 100, and a 90 degree slope having an infinite gradient.

Aspect maps were created in ArcGIS (Fig. 14) to highlight the direction a particular slope is facing, assigning a unique color to each 22.5 degree slope direction relative to north, highlighting the change in slope orientation. Circular cones show 8 equal-sized color sections radiating out from a central point, whereas an elongate ridge (if present) would show a long linear feature with only two colors present, since a ridge has only two dominant slopes. Figures 14-16 are aspect maps overlying a slope map, in order to define cone bases and shapes and make the most definitive tool for mapping the base of the cones. Most of the cones in this region have a circular pinwheel shape with equal color slices, indicating that a large number of the cones are

circular in shape and lack elongate features. All of the cones that displayed a circular pinwheel color scheme were mapped as circular cones.

Of the 40 elongate cones, 42.5% of them averaged Long Axis to Short Axis (LA:SA) ratios between 1.25 and 1.35, with 12.5% of the cone having a LA:SA ratio above 1.50. The long axes of elliptical cones were used to guide the trend of the alignment containing them. The average angular deviation between cone long axis azimuth and the azimuth of the alignment stayed within about 10-15 degrees, well within the requirements of the Paulsen and Wilson assessment method.

Twenty-one alignments were drawn in the Adare Basin, with each alignment containing between 2 and 7 cones, with 17 of the alignments containing at least one elongate cone. Over 50% of the alignments had lengths of 5-7 km, but alignments as short as 2 km and as long as 11 km were also present. The longer alignments contain a larger number of cones and elongate cones, but due to their great distances between cone centers, they still received low grades from the Paulsen and Wilson assessment method. The 21 alignments are mapped in Figures 19 and 20.

Standard deviation of the cone centers from a best fit line has the greatest variance. Six alignments have calculated standard deviations of <150m and are well within the limits defined in the Paulsen and Wilson method, whereas 4 alignments have deviations >300m and <450m with the largest reaching close to 700m.

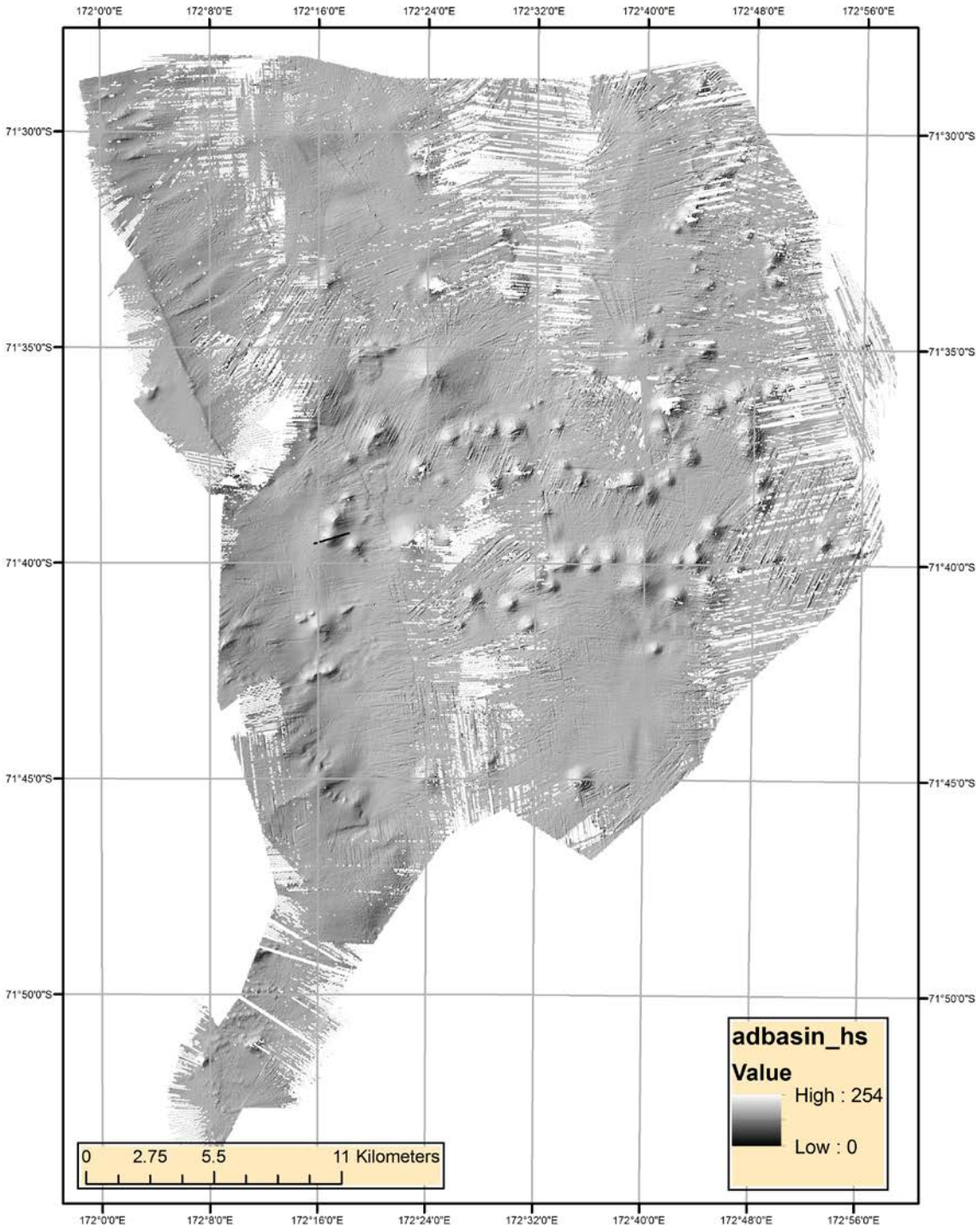

Figure 12: Hillshade Map of the Adare Basin Study Area with false illumination from a direction of 315 degrees

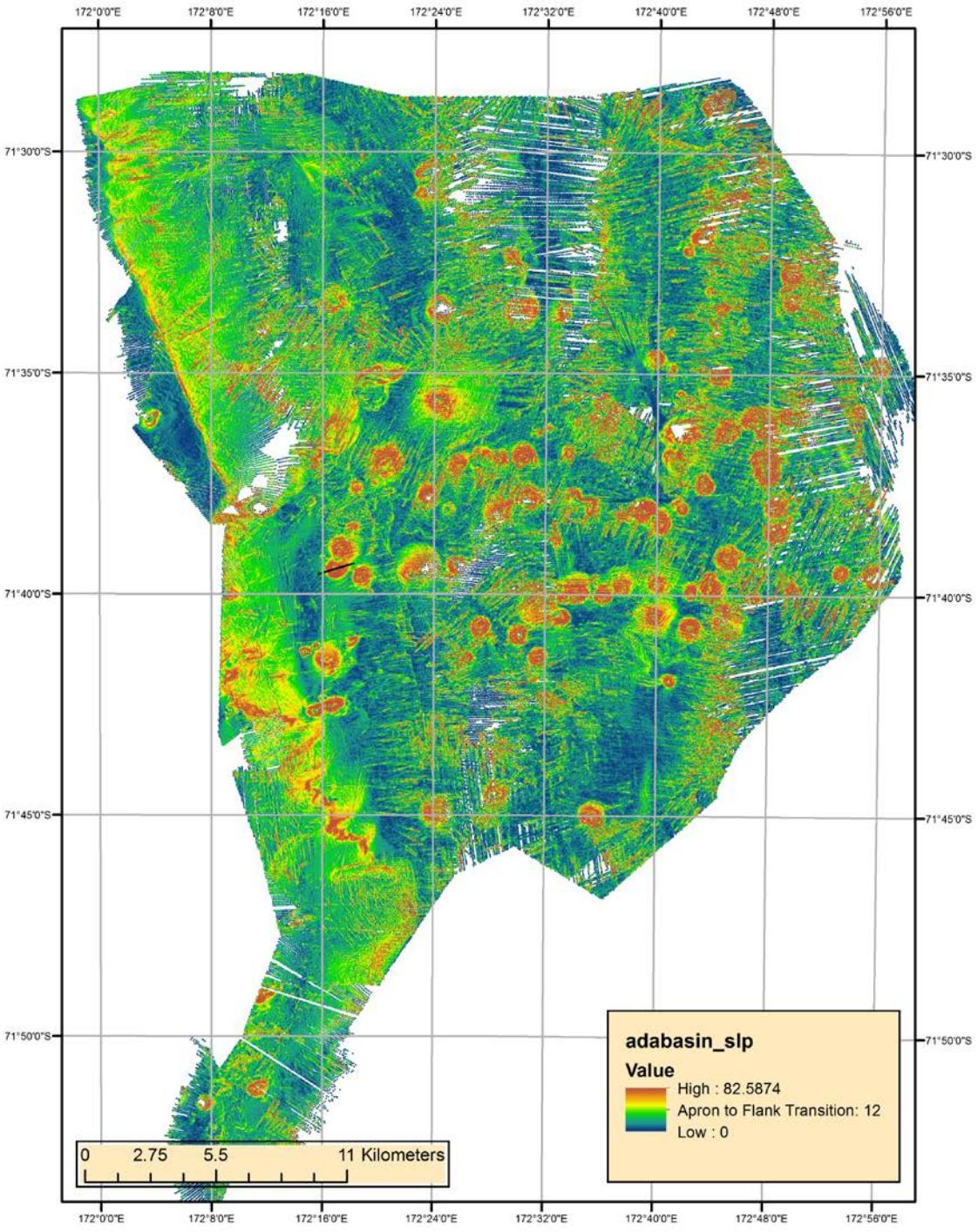

Figure 13: Slope Map of the Adare Basin Study Area, depicting slope gradient values

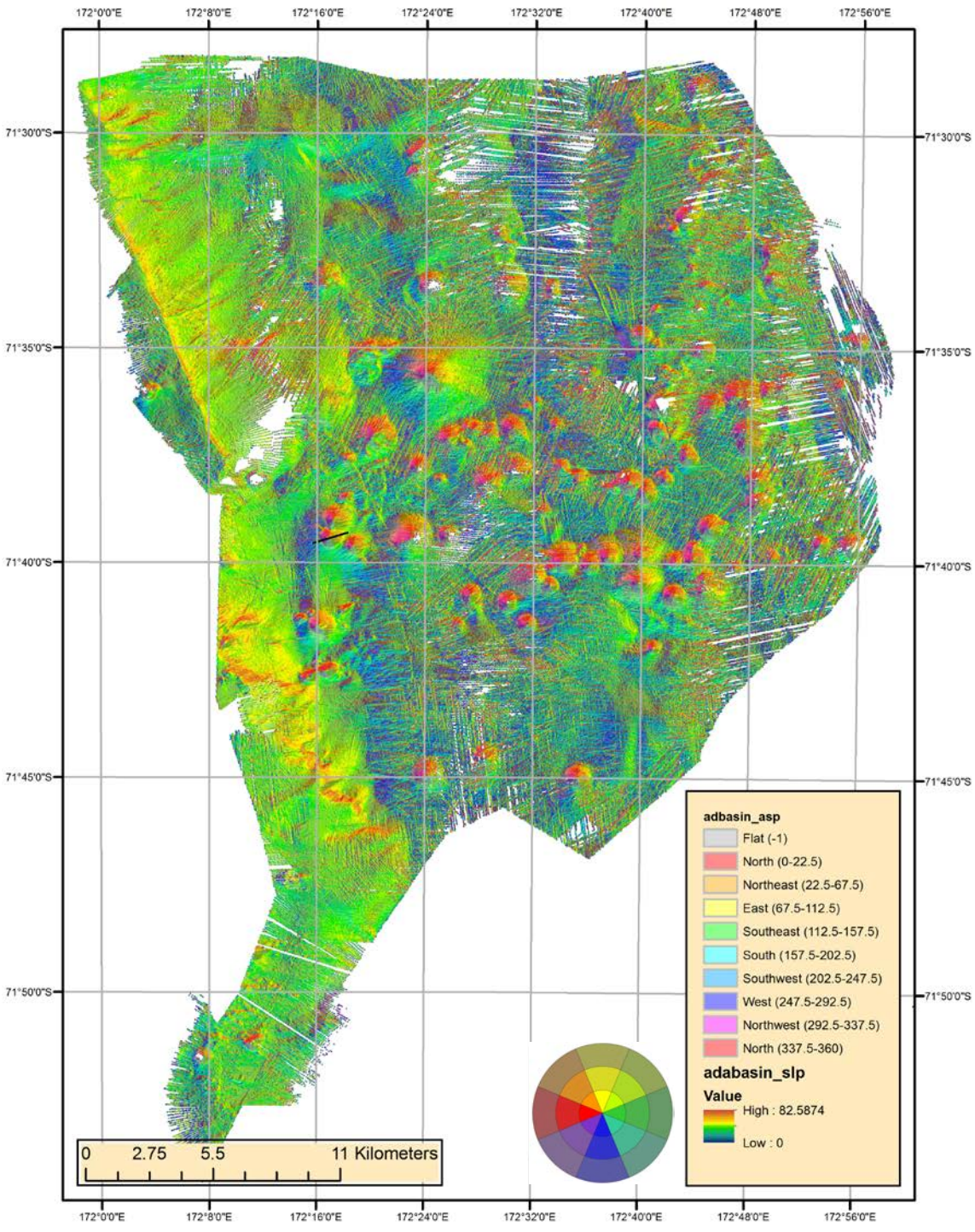

Figure 14: Slope Aspect Maps of the Adare Basin Study Area

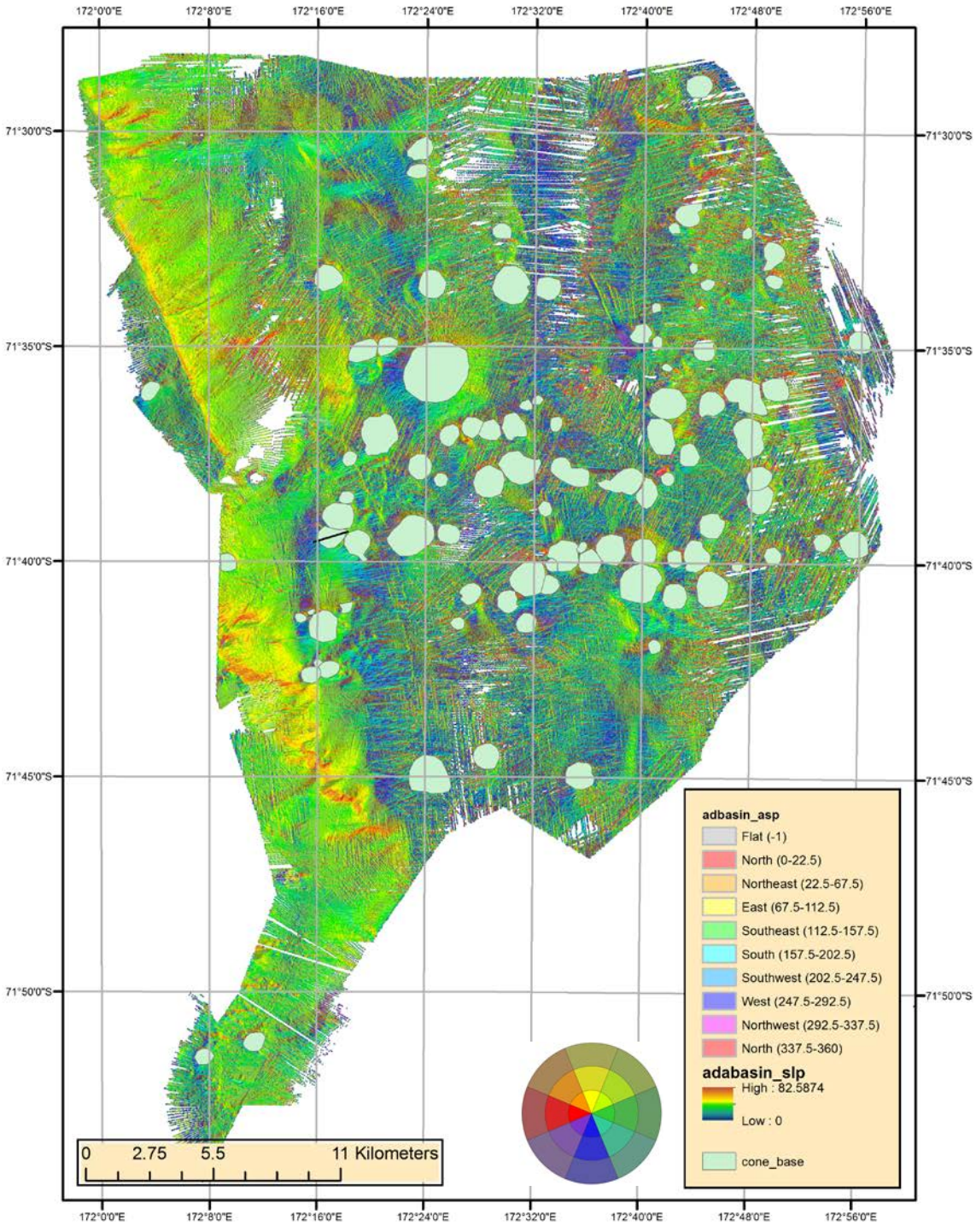

Figure 15: Slope Aspect Map with Cone Bases Mapped

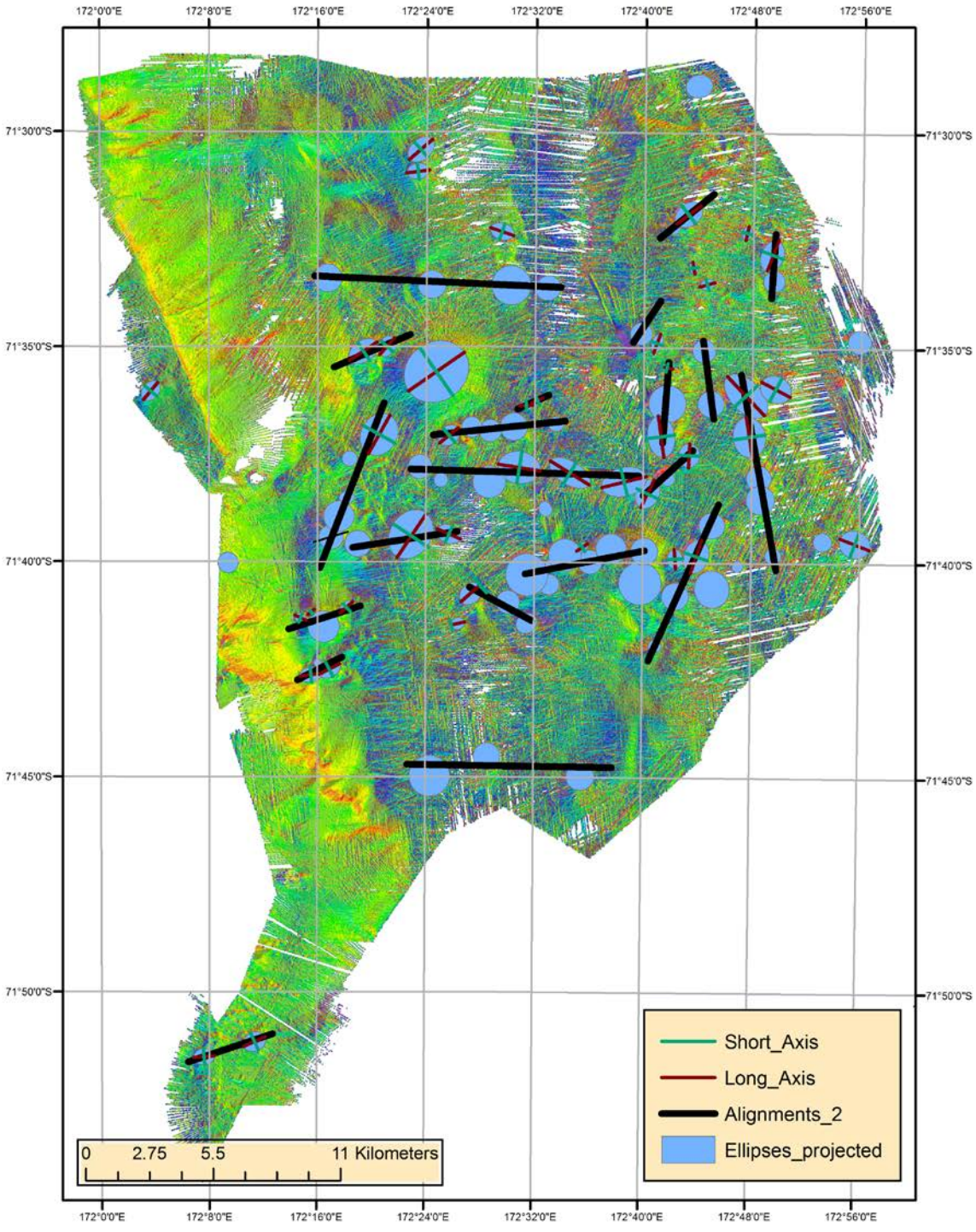

Figure 16: Slope Aspect Map with Alignments and Best Fit Ellipses with Long and Short Axes

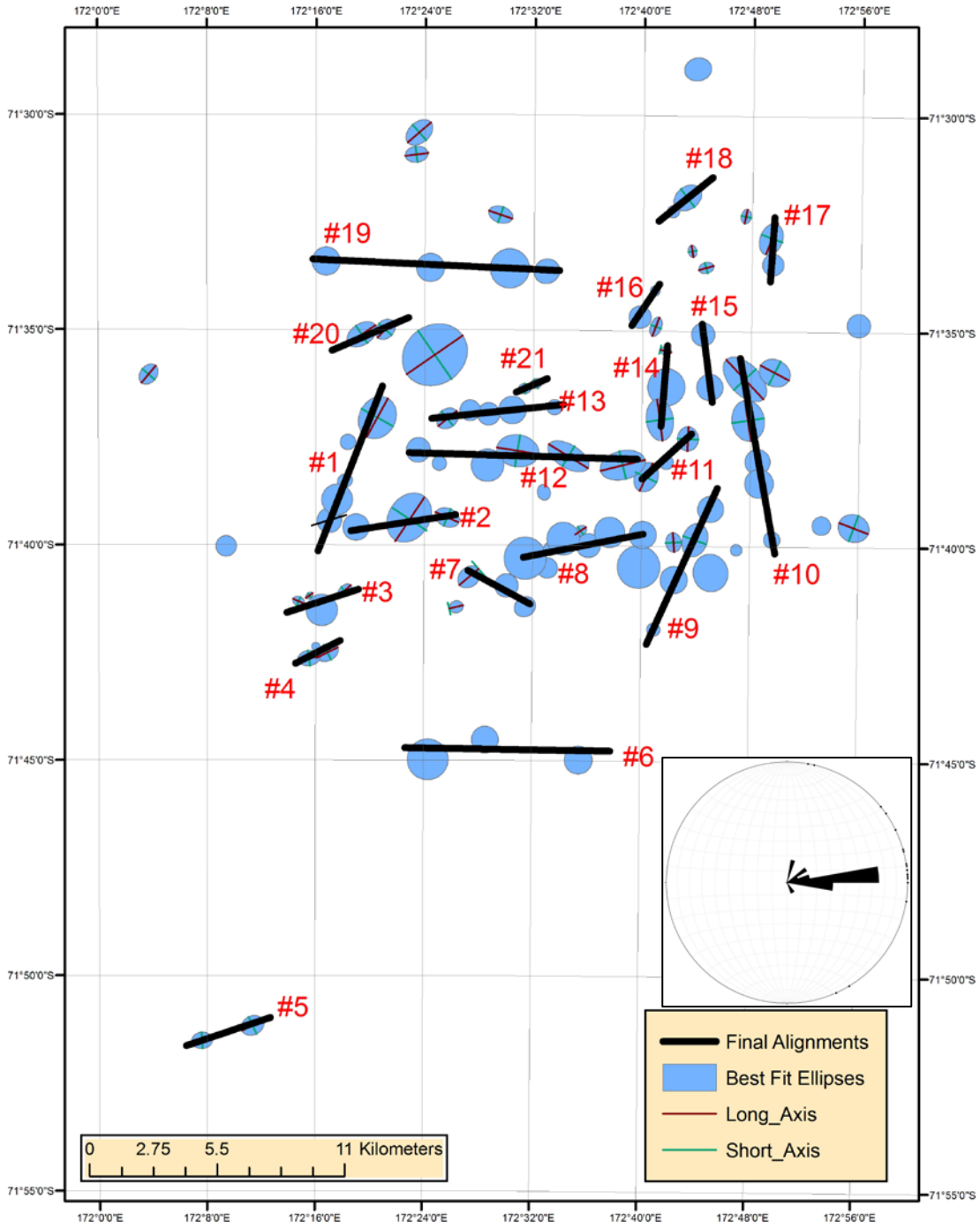

Figure 17: Alignment ID Map and Best Fit Ellipses with Long and Short Axes. The inset shows a rose diagram of alignment azimuth, with outer circle representing the compass direction of the alignments, showing the dominance of ~east-west alignments.

Discussion

All of the alignments drawn received a grade of C or less as estimated by the reliability assessment schedule of Paulsen and Wilson (2010), raising the question of whether the Adare Basin alignments can be used as markers for subsurface feeder dikes and, therefore, stress indicators. The size of the cones calls into question how well the Paulsen and Wilson assessment method works for submarine volcanic features in the Adare Basin. Many of the cones mapped in this study show diameters of 1-2 km, while the terrestrial scoria cones used in Paulsen and Wilson's characterizations were considerably smaller, ranging from 0.5 -1 km in diameter [Paulsen & Wilson, 2010]. With such difference in size, the spacing between vents limits in the Paulsen and Wilson assessment scheme does not apply in terms of the scale of the seafloor cones. The large spatial deviations of cones with respect to the best-fit alignment could also be a result of the difference in the size of the submarine cones compared with the scoria cones studied by Paulson and Wilson (2010). Modification of the Paulsen and Wilson assessment method may be required to calculate accurately the true reliability grades of submarine alignments, by means of a scaling factor that reflects the various sizes of cones present in a region. Given these factors, the alignment grades of C or lower does not appear to justify dismissing alignments as unreliable. An exception is if an alignment has only two cones and neither cone show signs of an elliptical shape, of which none exist in the set drawn.

The alignments show two trends: the dominant set of alignments have an E-W trend, and occur in the western and central portion of the study region, while another set of alignments show a N-S trend and occur in the eastern part of the region. With two sets of subperpendicular alignments, three possible interpretations can be made.

The first is that the magma moving upwards through the crust travelled along two pre-existing sets of fractures in the crust under an isotropic state of crustal stress, and both sets of alignments formed at the same time. This means that the two sets of subperpendicular fractures formed before the cones were created.

The second is that both sets of fractures formedover the same interval of time, and during the ongoing volcanism in the region, the least principal stress in the crust changed 90 degrees, allowing a second set of fractures to form, and therefore the second alignment set. This occurs as magma intrudes to the surface and creates a set of linear volcanic features, such as dikes. As these dikes from perpendicular to the greatest principal stress, the pressure and heating of the magma changes the orientation of stress in the crust so that the least principal stress orientation now becomes the greatest principal stress orientation, resulting in a new set of volcanic features forming perpendicular to the older features (McCarthy and Thompson, 1988).

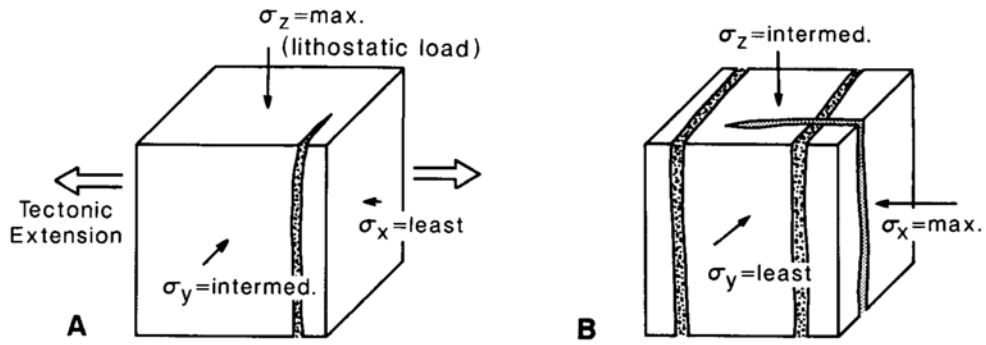

Figure 18: Diagram of the principal stress in the crust changing orientation due to the force of pressurized magma expanding, increasing the stress that is perpendicular to volcanic dikes, resulting in the least principal stress becoming the greatest principal stress, and causing the orientation of surface volcanic feature to change with it (McCarthy and Thompson, 1988).

The third possibility is that the two set of alignments formed at different times, under two separate stress states that existed at near-perpendicular angles to each other. Dates from the

cones in the region indicate an age of 2.76-3.12 Ma, which shows that the cones in the study area all formed from the same set of volcanic events. This means the likelihood of these two alignments sets having formed at different times is low.

Granot et al. (2010) mapped fault trends in the southern part of the Adare rift basin to the east and northeast of the study area. Normal faults have north to north-northeast trends close to the volcanic field, subparallel to the volcanic alignments found in the easternmost portion of the study region. Granot et al. (2010) documented Pliocene faulting, interpreted to have near-zero associated extension, coeval with Pliocene – recent volcanism throughout the Adare Basin region. Dates from seamounts within the current study area range between 2.76 – 3.12 Ma (Panter and Castillo, 2007), but there is no information available linking these dates to specific mapped cones. Therefore it is not possible to test the hypothesis that the E-W and N-S alignments formed at different times.

The combination of agreement in timing and overall continuity with the regional structure of the Adare Basin Rift leads to the hypothesis that these two sets of alignments formed at separate times, with the eastern set of alignments forming under the same stress state that created the overall N-S trending volcanic and structural features seen in the Adare Basin today, while the E-W trending volcanic features formed as a result of the stress stage in the crust switching due to the pressure and heating of magma in the crust, resulting in the perpendicular pattern of alignments shown.

Conclusion

Overall, 93 cones were mapped in the Adare Basin, with 40 cones showing varying degrees of elliptical shape and the other 53 having a circular shape. The average slope of the cone flanks varies between 38-41 degrees, with values of the cone aprons ranging from 13-17 degrees, as shown in Figures 8-10 and in Appendix A. Most of the cones have a diameter that ranges from 900 to 1300 meters across, although cones both smaller and larger than that are present. Over 70% of the cones in study region have heights between 150m and 250m, with a handful of cones with heights greater than 250m or less than 150m.

Two alignment trends are mapped, with one set of 12 alignments having an E-W trend, and another set of 4 alignments having a ~N-S trend. The remaining 5 alignments have intermediate azimuth directions near to the E-W trend. These two separate sets of alignments have some geographic separation, with E-W trends in the western and central regions, and N-S trends in the eastern region. Considering the proximity of the eastern, N-S trending alignments to the rift faults mapped in the Adare Basin to the east, it's possible that these few N-S trending alignments are related to the rift structures, and therefore the extensional stress regime that existed in the Adare Basin. Combined with the dates of the cones that have them all being formed from 2.76-3.12 Ma, it seems that the most plausible conclusion is that the two sets of alignments formed at separate times under different stress regimes, with the more eastern N-S alignments related to rifting in the Adare Basin, and the E-W trending alignments having formed from a switch of the least and greatest principal stress in the crust from the pressure and heating of the intruding magma, giving the perpendicular series of alignments shown.

Further study in the area would be to confine the dates of each volcanic cone in order to identify if there are two separate series of cones based on age, and if they correlate to the alignments drawn in this study.

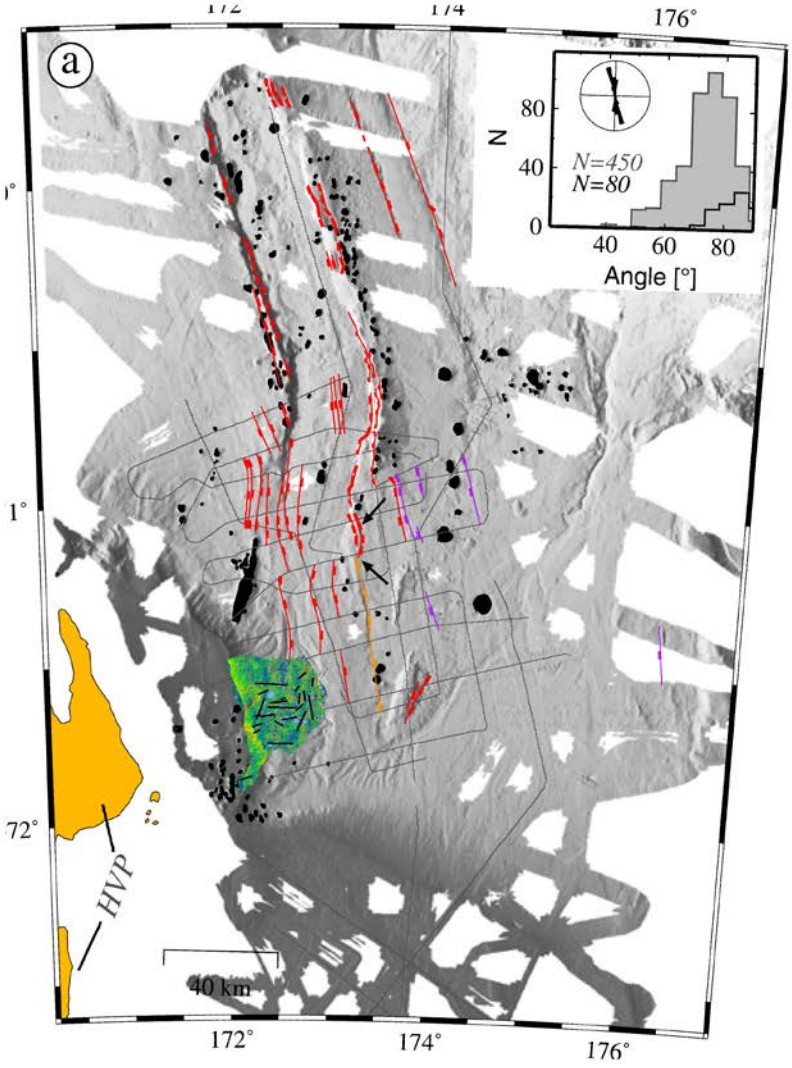

Figure 19: Map of the Adare Basin with normal faults highlighted. Slope map with alignments and best-fit ellipses overlaid [Modified Granot et al., 2010]

References

Anderson, E.M. (1951). *The Dynamics of Faulting and Dyke Formation with Applications to Britain*, 2nd Edition, Oliver and Boyd, Edinbough, p. 206.

Behrendt, J.C et al. (1991). Geophysical studies of the West Antarctic Rift System, *Tectonics*, 10 (6), pp. 1257-1273.

Behrendt, J.C. (1999). Crustal and lithospheric structure of the West Antarctic Rift System from geophysical investigations – a review, *Global and Planetary Change*, 23(1-4), pp. 25-44.

Cande, S.C., J.M. Stock, R.D. Müller, and T. Ishihara (2000)., Cenozoic motion between East and West Antarctica. *Nature*, 404, 145-150

Fitzgerald, P. (2002). Tectonics and landscape evolution of the Antarctic plate since the breakup of
Gondwana, with an emphasis on the West Antarctic Rift System and the
Transantarctic Mountains, *Royal Society of New Zealand Bulletin*, 35, pp. 453-469.

Granot, R. et al. (2010). Postspreading rifting in the Adare Basin, Antarctica: Regional tectonic consequences, *Geochemistry Geophysics Geosystems*, *11* (8), pp. 1-29.

Kyle, P.R. (1990). A. McMurdo Volcanic Group Western Ross Embayment, *Volcanoes of the Antarctic Plate and Southern Oceans*, 48, pp. 19-35.

McCarthy, J. and Thompson, G.A. (1988). Seismic imaging of the extended crust with emphasis on the western United States, *Geological Society of America Bulletin, 100* (9), pp. 1361-1374.

Nakamura, K. (1977). Volcanoes as possible indicators of tectonic stress orientation – principle and proposal, *Journal of Volcanology and Geothermal Research,* 2, pp. 1-16.

Panter, K.S. & Castillo P. (2007) Petrogenesis and source of lavas from seamounts in the Adare Basin, Western Ross Sea: Implications for the origin of Cenozoic magmatism in Antarctica, *U.S. Geological Survey and the National Academies*, 1047, pp.1-4.

Paulsen, T.S. & Wilson, T.J. (2010). New criteria for systematic mapping and reliability assessment of monogenetic volcanic vent alignments and elongate volcanic vents for crustal analysis, *Tectonophysics, 482*, pp.16-28.

Van der Pluijm, B.A. (2004) *Earth Structure*. New York, NY: W.W. Norton & Company Ltd.

Appendix A: Cone Analysis Profiles

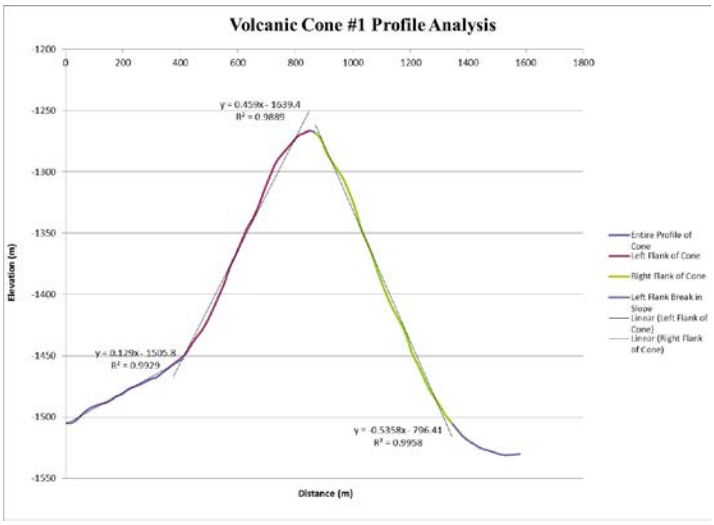

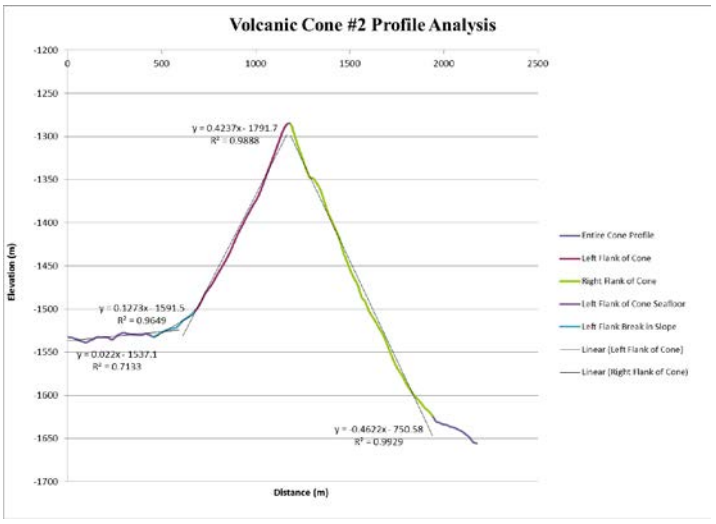

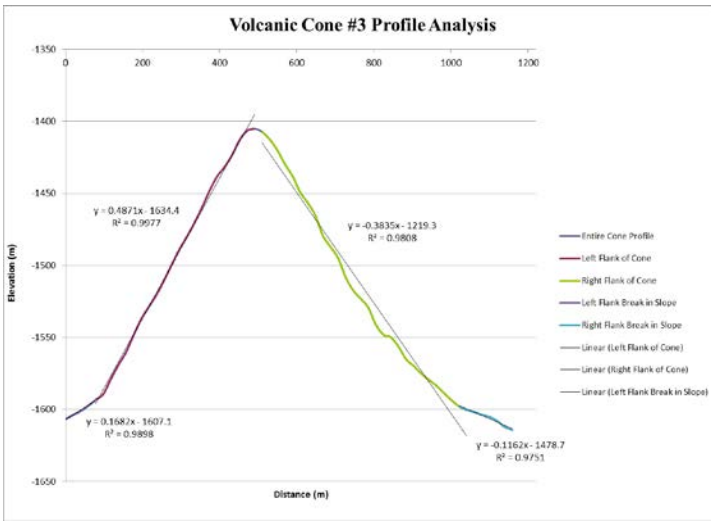

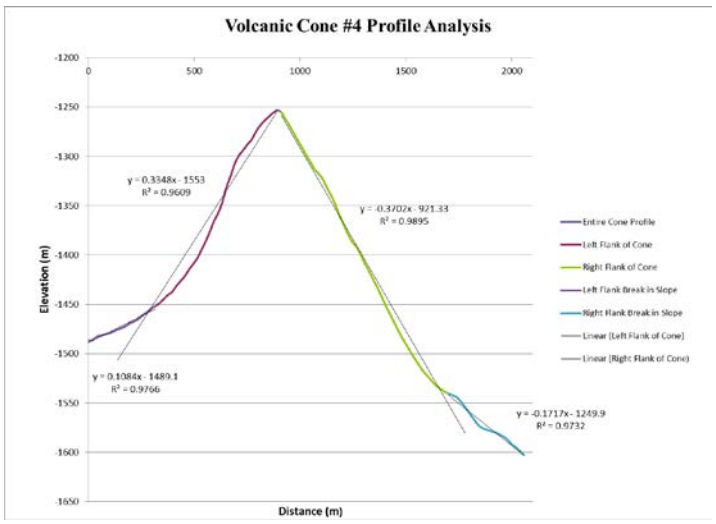

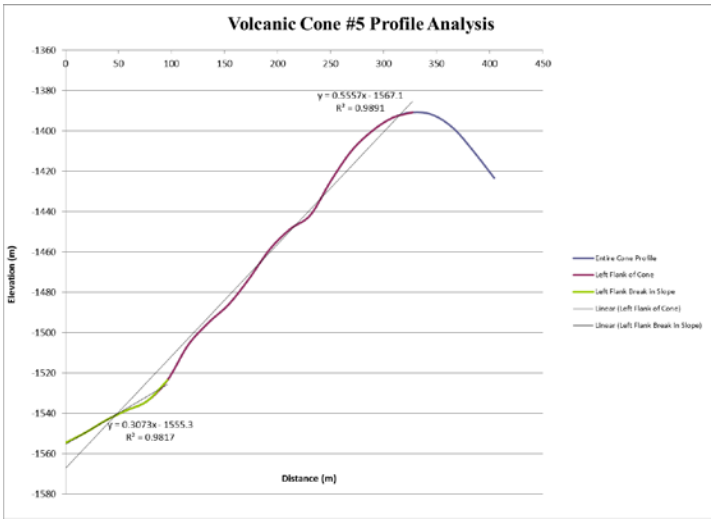

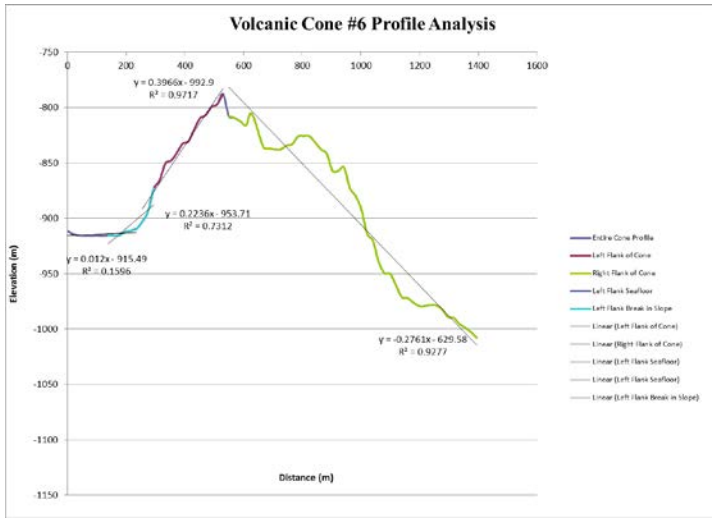

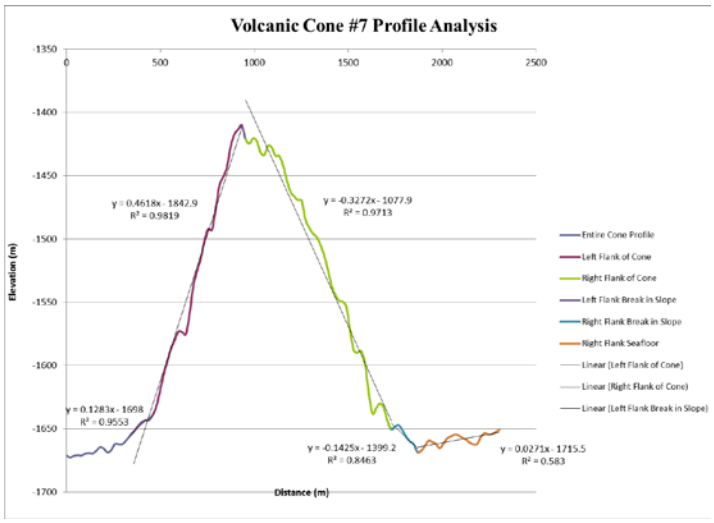
Volcanic Cone #7 Profile Analysis
y = 0.4618x - 1842.9
R² = 0.9819
y = -0.3272x - 1077.9
R² = 0.9713
y = 0.1283x - 1698
R² = 0.9553
y = -0.1425x - 1399.2
R² = 0.8463
y = 0.0271x - 1715.5
R² = 0.583
Elevation (m)
Distance (m)
Entire Cone Profile
Left Flank of Cone
Right Flank of Cone
Left Flank Break in Slope
Right Flank Break in Slope
Right Flank Seafloor
Linear (Left Flank of Cone)
Linear (Right Flank of Cone)
Linear (Left Flank Break in Slope)

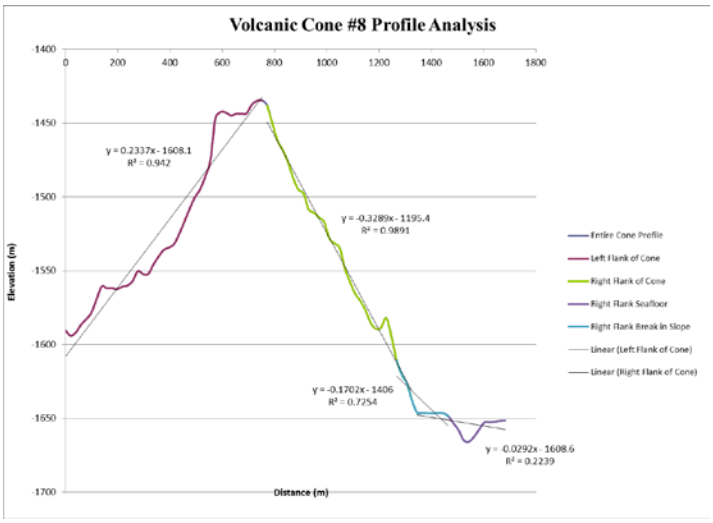
Volcanic Cone #8 Profile Analysis
y = 0.2337x - 1608.1
R² = 0.942
y = -0.3289x - 1195.4
R² = 0.9891
y = -0.1702x - 1406
R² = 0.7254
y = -0.0292x - 1608.6
R² = 0.2239
Elevation (m)
Distance (m)
Entire Cone Profile
Left Flank of Cone
Right Flank of Cone
Right Flank Seafloor
Right Flank Break in Slope
Linear (Left Flank of Cone)
Linear (Right Flank of Cone)

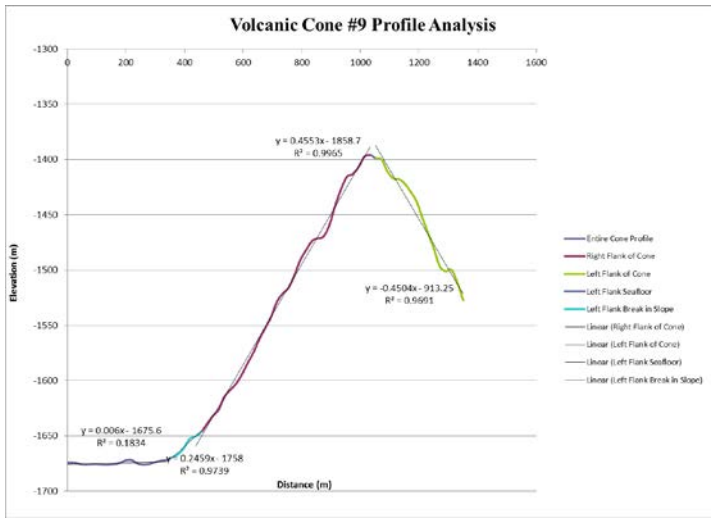
Volcanic Cone #9 Profile Analysis
y = 0.4553x - 1858.7
R² = 0.9965
y = -0.4504x - 913.25
R² = 0.9691
y = 0.006x - 1675.6
R² = 0.1834
y = 0.2459x - 1758
R² = 0.9739
Elevation (m)
Distance (m)
Entire Cone Profile
Right Flank of Cone
Left Flank of Cone
Left Flank Seafloor
Left Flank Break in Slope
Linear (Right Flank of Cone)
Linear (Left Flank of Cone)
Linear (Left Flank Seafloor)
Linear (Left Flank Break in Slope)

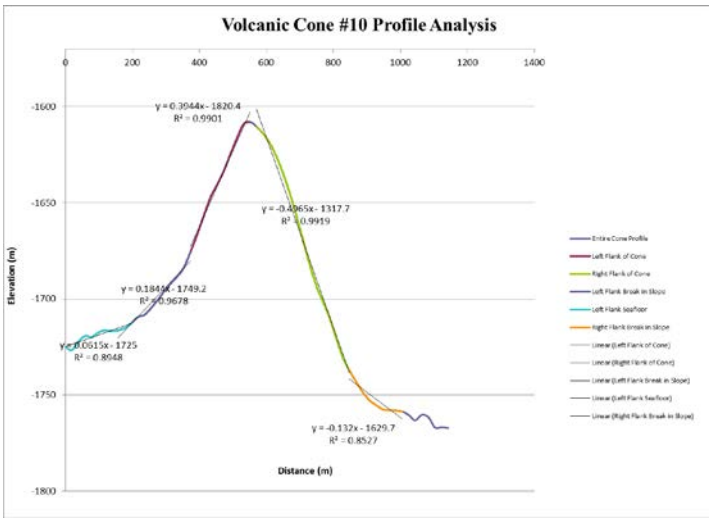
Volcanic Cone #10 Profile Analysis
y = 0.3944x - 1820.4
R² = 0.9901
y = -0.4965x - 1317.7
R² = 0.9919
y = 0.1844x - 1749.2
R² = 0.9678
y = 0.0615x - 1725
R² = 0.8948
y = -0.132x - 1629.7
R² = 0.8527
Elevation (m)
Distance (m)

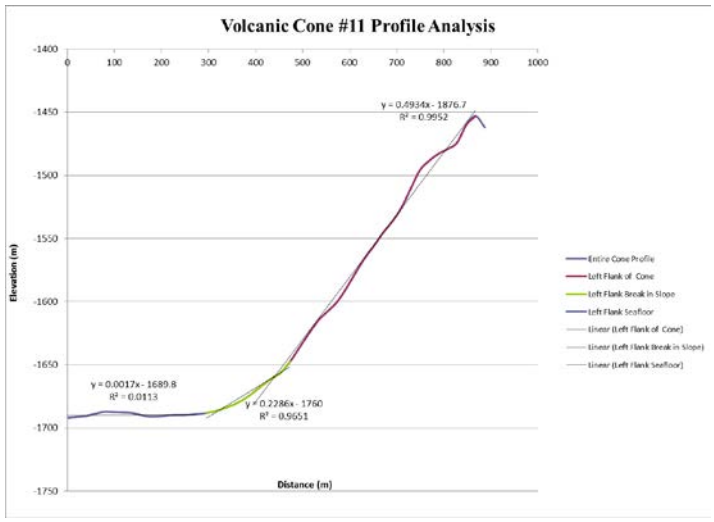
Volcanic Cone #11 Profile Analysis
y = 0.6934x - 1876.7
R² = 0.9952
y = 0.0017x - 1689.8
R² = 0.0113
y = 0.2286x - 1760
R² = 0.9651
Elevation (m)
Distance (m)
Entire Cone Profile
Left Flank of Cone
Left Flank Break in Slope
Left Flank Seafloor
Linear (Left Flank of Cone)
Linear (Left Flank Break in Slope)
Linear (Left Flank Seafloor)

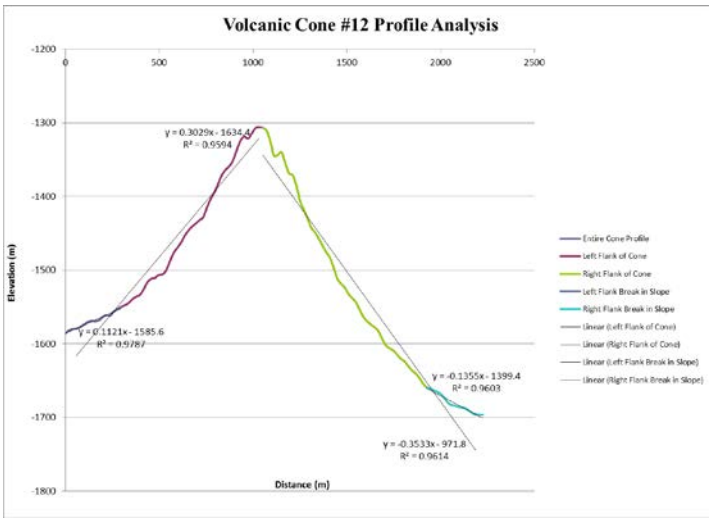
Volcanic Cone #12 Profile Analysis
y = 0.3029x - 1634.4
R² = 0.9594
y = 0.1121x - 1585.6
R² = 0.9787
y = -0.1355x - 1399.4
R² = 0.0603
y = -0.3533x - 971.8
R² = 0.9614
Elevation (m)
Distance (m)
Entire Cone Profile
Left Flank of Cone
Right Flank of Cone
Left Flank Break in Slope
Right Flank Break in Slope
Linear (Left Flank of Cone)
Linear (Right Flank of Cone)
Linear (Left Flank Break in Slope)
Linear (Right Flank Break in Slope)

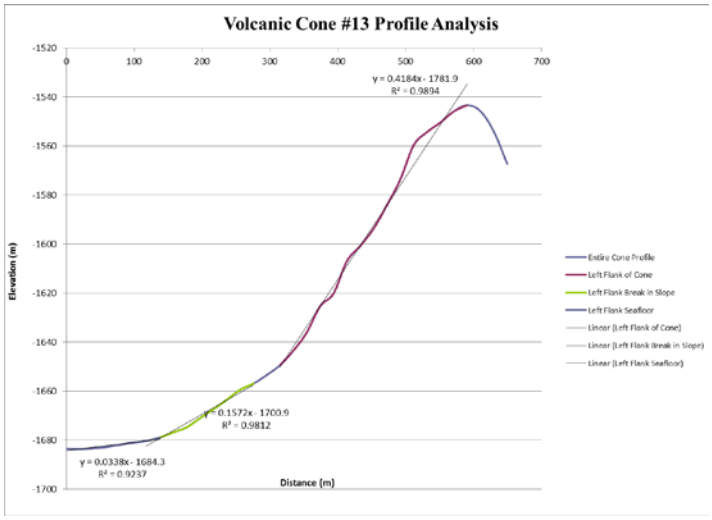
Volcanic Cone #13 Profile Analysis
y = 0.4184x - 1781.9
R² = 0.9894
y = 0.1572x - 1700.9
R² = 0.9812
y = 0.0338x - 1684.3
R² = 0.9237
Elevation (m)
Distance (m)
Entire Cone Profile
Left Flank of Cone
Left Flank Break in Slope
Left Flank Seafloor
Linear (Left Flank of Cone)
Linear (Left Flank Break in Slope)
Linear (Left Flank Seafloor)

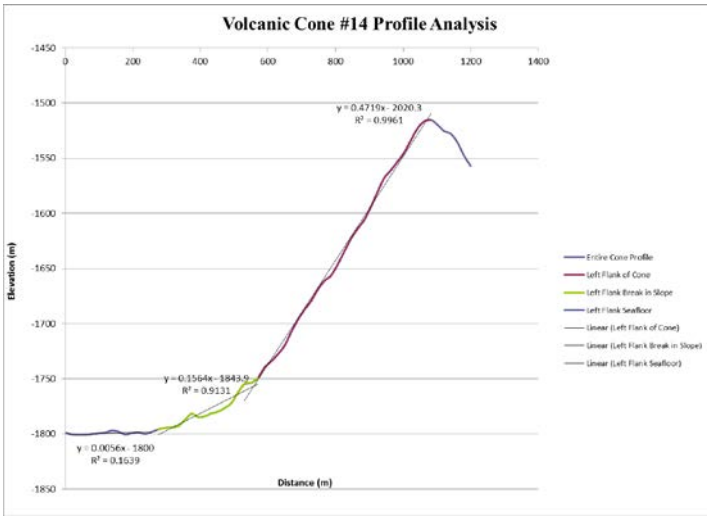
Volcanic Cone #14 Profile Analysis
y = 0.4719x - 2020.3
R² = 0.9961
y = 0.1564x - 1843.9
R² = 0.9131
y = 0.0056x - 1800
R² = 0.1639
Elevation (m)
Distance (m)
Entire Cone Profile
Left Flank of Cone
Left Flank Break in Slope
Left Flank Seafloor
Linear (Left Flank of Cone)
Linear (Left Flank Break in Slope)
Linear (Left Flank Seafloor)

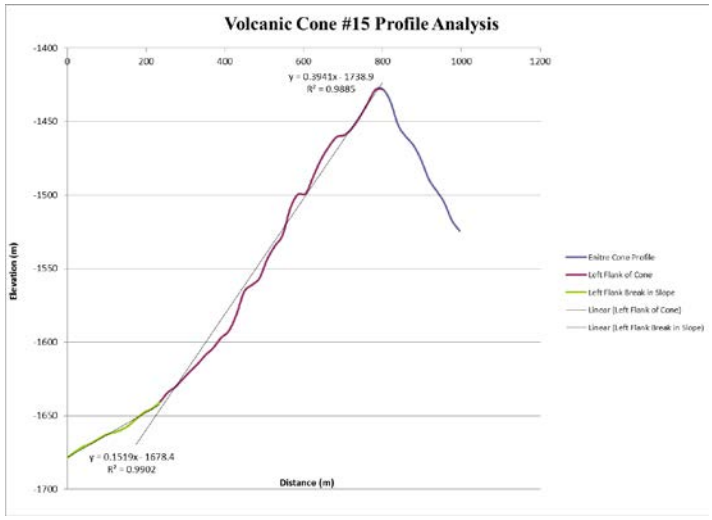
Volcanic Cone #15 Profile Analysis
y = 0.3941x - 1738.9
R² = 0.9885
y = 0.1519x - 1678.4
R² = 0.9902
Elevation (m)
Distance (m)
Entire Cone Profile
Left Flank of Cone
Left Flank Break in Slope
Linear (Left Flank of Cone)
Linear (Left Flank Break in Slope)

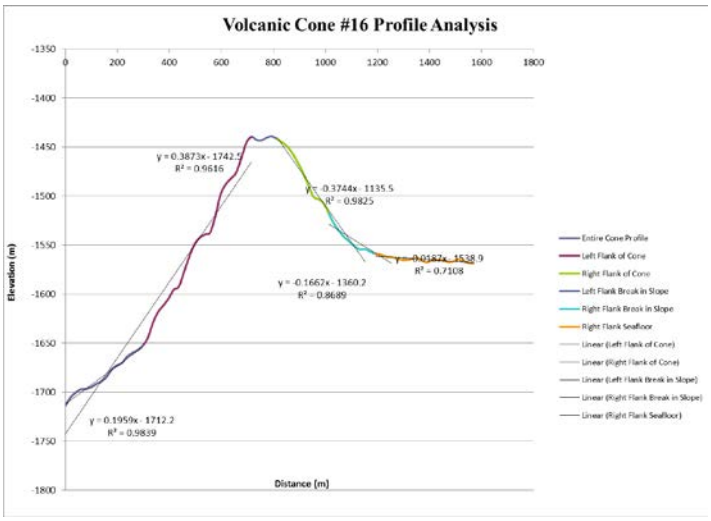
Volcanic Cone #16 Profile Analysis
y = 0.3744x - 1135.5
R² = 0.9825
y = -0.1667x - 1360.2
R² = 0.8689
y = 0.1959x - 1712.2
R² = 0.9839
Elevation (m)
Distance (m)
Entire Cone Profile
Left Flank of Cone
Right Flank of Cone
Left Flank Break in Slope
Right Flank Break in Slope
Right Flank Seafloor
Linear (Left Flank of Cone)
Linear (Right Flank of Cone)
Linear (Left Flank Break in Slope)
Linear (Right Flank Break in Slope)
Linear (Right Flank Seafloor)

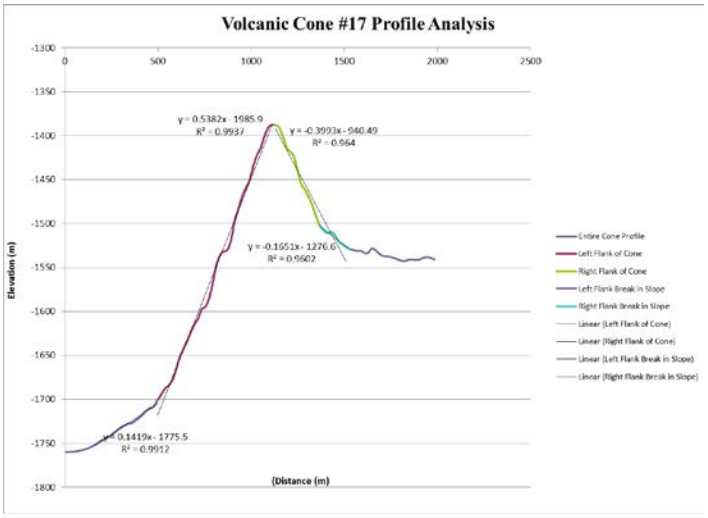
Volcanic Cone #17 Profile Analysis
y = 0.5382x - 1985.9
R² = 0.9937
y = -0.3993x - 940.49
R² = 0.964
y = -0.1651x - 1276.6
R² = 0.9602
y = 0.1419x - 1775.5
R² = 0.9912
Elevation (m)
(Distance (m)
Entire Cone Profile
Left Flank of Cone
Right Flank of Cone
Left Flank Break in Slope
Right Flank Break in Slope
Linear (Left Flank of Cone)
Linear (Right Flank of Cone)
Linear (Left Flank Break in Slope)
Linear (Right Flank Break in Slope)

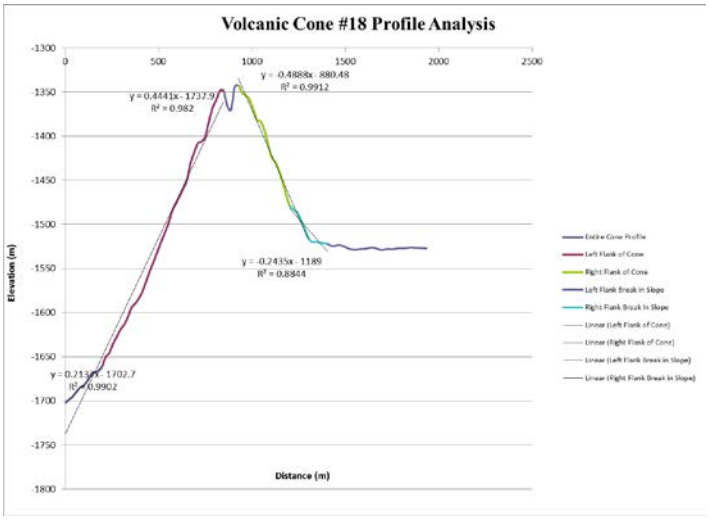
Volcanic Cone #18 Profile Analysis
y = 0.4888x - 880.48
R² = 0.9912
y = 0.4441x - 1737.9
R² = 0.982
y = -0.2435x - 1189
R² = 0.8844
Elevation (m)
Distance (m)
Entire Cone Profile
Left Flank of Cone
Right Flank of Cone
Left Flank Break in Slope
Right Flank Break in Slope
Linear (Left Flank of Cone)
Linear (Right Flank of Cone)
Linear (Left Flank Break in Slope)
Linear (Right Flank Break in Slope)

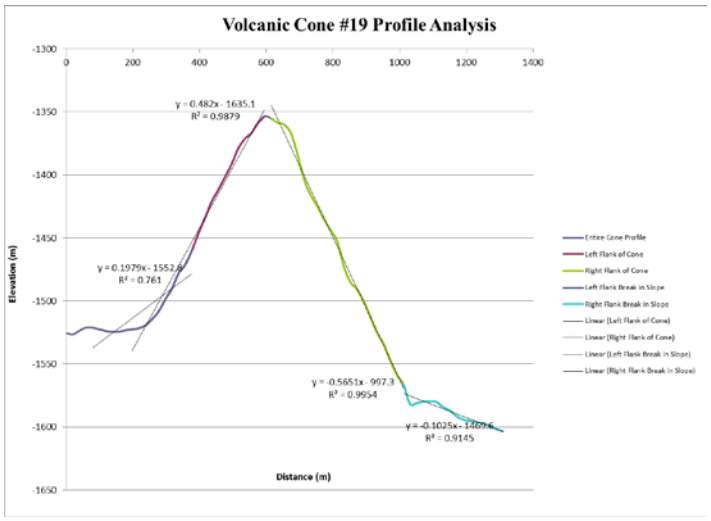
Volcanic Cone #19 Profile Analysis
y = 0.482x - 1635.1
R² = 0.9879
y = 0.1979x - 1552.6
R² = 0.761
y = -0.5651x - 907.3
R² = 0.9954
y = -0.1025x - 1469.6
R² = 0.9145
Elevation (m)
Distance (m)
Entire Cone Profile
Left Flank of Cone
Right Flank of Cone
Left Flank Break in Slope
Right Flank Break in Slope
Linear (Left Flank of Cone)
Linear (Right Flank of Cone)
Linear (Left Flank Break in Slope)
Linear (Right Flank Break in Slope)

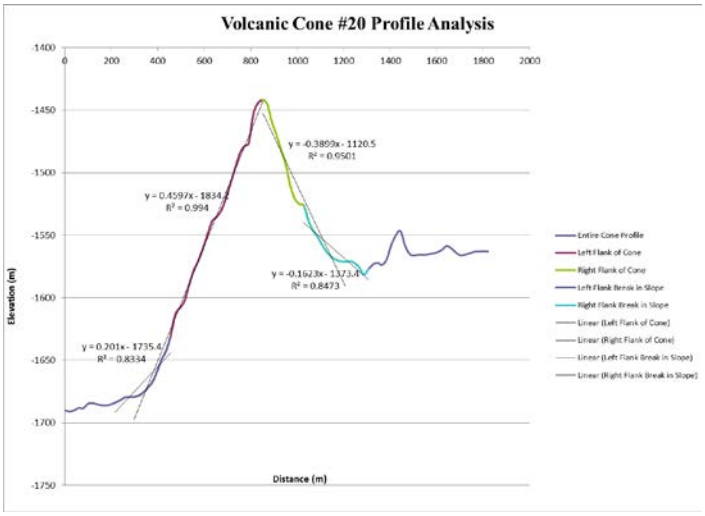
Volcanic Cone #20 Profile Analysis
y = -0.3899x - 1120.5
R² = 0.9501
y = 0.4597x - 1834.2
R² = 0.994
y = -0.1623x - 1373.4
R² = 0.8473
y = 0.201x - 1735.4
R² = 0.8334
Elevation (m)
Distance (m)
Entire Cone Profile
Left Flank of Cone
Right Flank of Cone
Left Flank Break in Slope
Right Flank Break in Slope
Linear (Left Flank of Cone)
Linear (Right Flank of Cone)
Linear (Left Flank Break in Slope)
Linear (Right Flank Break in Slope)

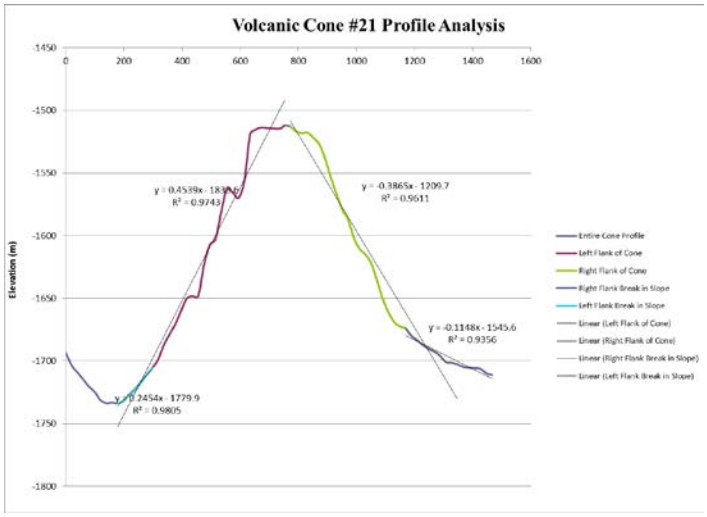
Volcanic Cone #21 Profile Analysis
y = 0.4539x - 1839.6
R² = 0.9743
y = -0.3865x - 1209.7
R² = 0.9611
y = -0.1148x - 1545.6
R² = 0.9356
y = 0.2454x - 1779.9
R² = 0.9805
Elevation (m)
Entire Cone Profile
Left Flank of Cone
Right Flank of Cone
Right Flank Break in Slope
Left Flank Break in Slope
Linear (Left Flank of Cone)
Linear (Right Flank of Cone)
Linear (Right Flank Break in Slope)
Linear (Left Flank Break in Slope)

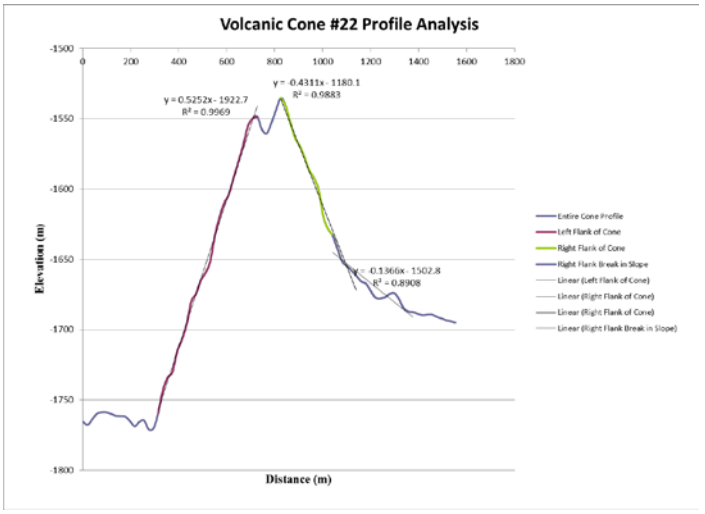
Volcanic Cone #22 Profile Analysis
y = -0.4311x - 1180.1
R² = 0.9883
y = 0.5252x - 1922.7
R² = 0.9969
y = -0.1366x - 1502.8
R² = 0.8908
Elevation (m)
Distance (m)
Entire Cone Profile
Left Flank of Cone
Right Flank of Cone
Right Flank Break in Slope
Linear (Left Flank of Cone)
Linear (Right Flank of Cone)
Linear (Right Flank Break in Slope)

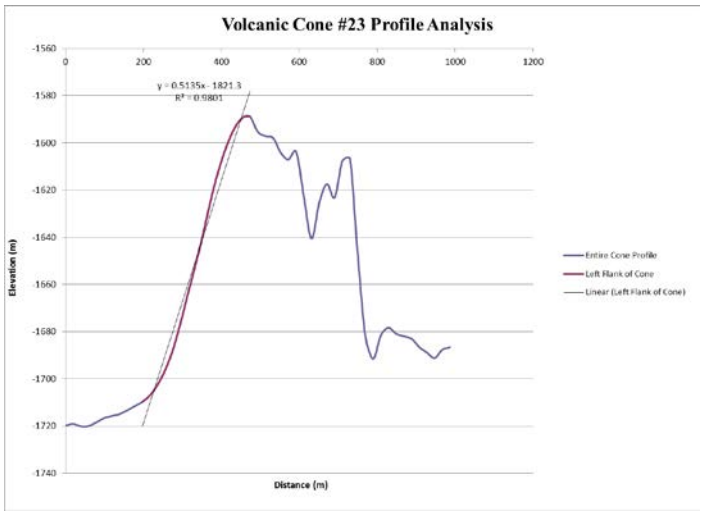
Volcanic Cone #23 Profile Analysis
y = 0.5135x - 1821.3
R² = 0.9801
Elevation (m)
Distance (m)
Entire Cone Profile
Left Flank of Cone
Linear (Left Flank of Cone)

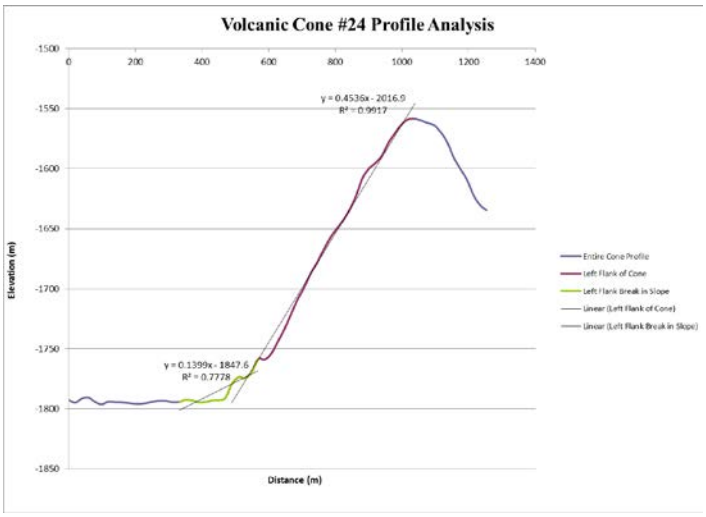
Volcanic Cone #24 Profile Analysis
y = 0.4536x - 2016.9
R² = 0.9917
y = 0.1399x - 1847.6
R² = 0.7778
Elevation (m)
Distance (m)
Entire Cone Profile
Left Flank of Cone
Left Flank Break in Slope
Linear (Left Flank of Cone)
Linear (Left Flank Break in Slope)

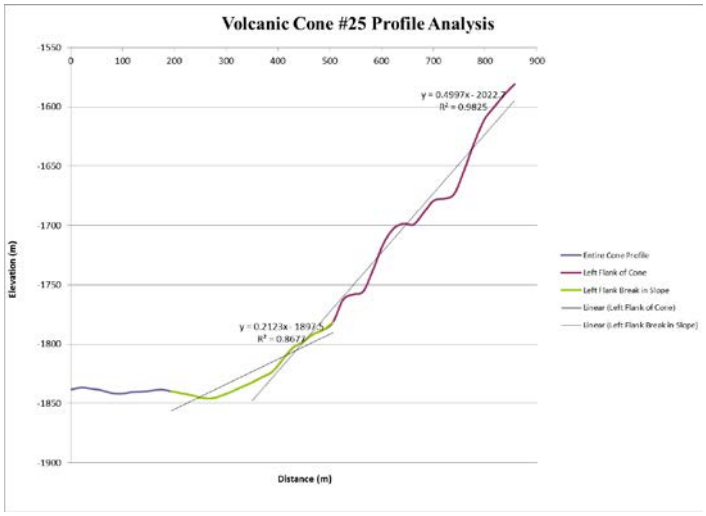
Volcanic Cone #25 Profile Analysis
Elevation (m)
Distance (m)
y = 0.4997x - 2022.2
R² = 0.9825
y = 0.2123x - 1897.5
R² = 0.8677
Entire Cone Profile
Left Flank of Cone
Left Flank Break in Slope
Linear (Left Flank of Cone)
Linear (Left Flank Break in Slope)

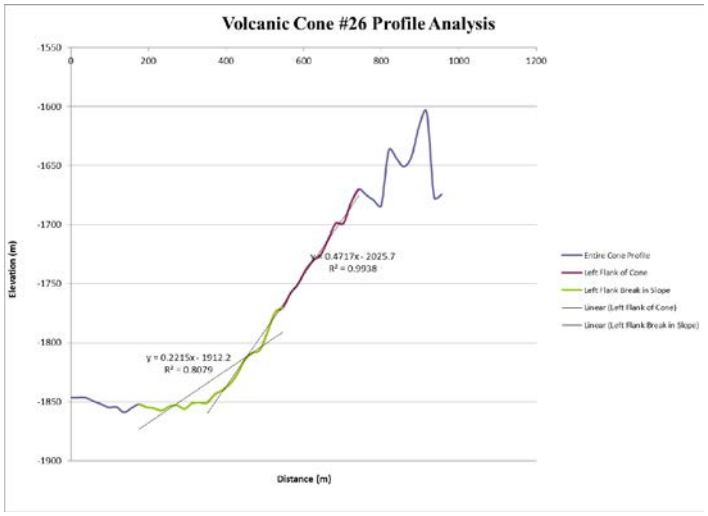
Volcanic Cone #26 Profile Analysis
Elevation (m)
Distance (m)
y = 0.4717x - 2025.7
R² = 0.9938
y = 0.2215x - 1912.2
R² = 0.8079
Entire Cone Profile
Left Flank of Cone
Left Flank Break in Slope
Linear (Left Flank of Cone)
Linear (Left Flank Break in Slope)

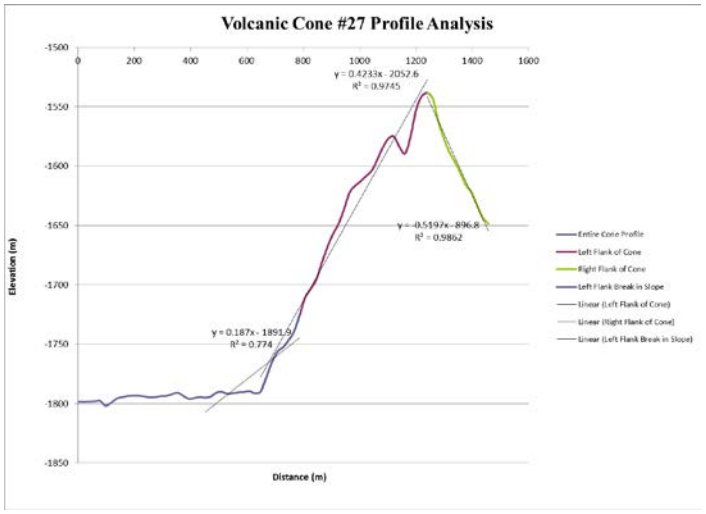
Volcanic Cone #27 Profile Analysis
Elevation (m)
Distance (m)
y = 0.4233x - 2052.6
R² = 0.9745
y = -0.5197x - 896.8
R² = 0.9862
y = 0.187x - 1891.9
R² = 0.774
Entire Cone Profile
Left Flank of Cone
Right Flank of Cone
Left Flank Break in Slope
Linear (Left Flank of Cone)
Linear (Right Flank of Cone)
Linear (Left Flank Break in Slope)

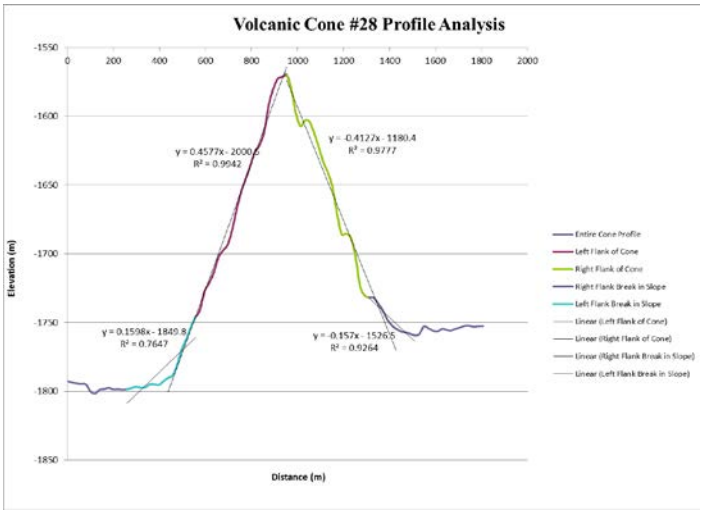
Volcanic Cone #28 Profile Analysis
Elevation (m)
Distance (m)
y = 0.4577x - 2000.6
R² = 0.9942
y = -0.4127x - 1180.4
R² = 0.9777
y = 0.1598x - 1849.8
R² = 0.7647
y = -0.157x - 1526.5
R² = 0.9264
Entire Cone Profile
Left Flank of Cone
Right Flank of Cone
Right Flank Break in Slope
Left Flank Break in Slope
Linear (Left Flank of Cone)
Linear (Right Flank of Cone)
Linear (Right Flank Break in Slope)
Linear (Left Flank Break in Slope)

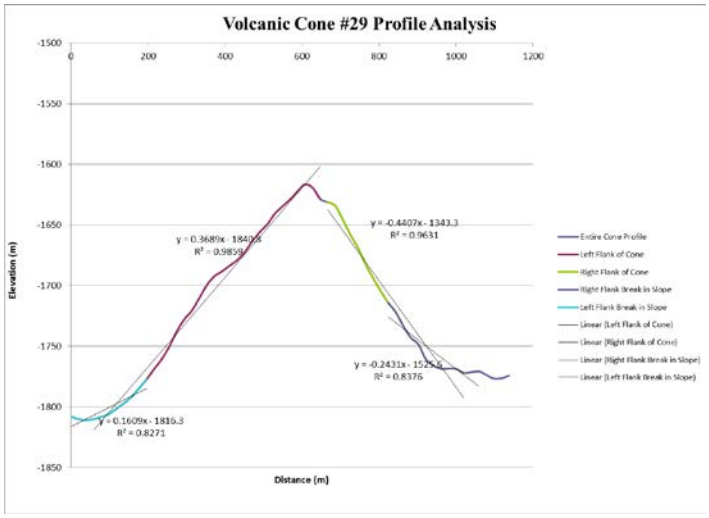
Volcanic Cone #29 Profile Analysis
Elevation (m)
Distance (m)
y = 0.3689x - 1840.8
R² = 0.9839
y = -0.4407x - 1343.3
R² = 0.9631
y = -0.2431x - 1525.9
R² = 0.8375
y = 0.1609x - 1816.3
R² = 0.8271
Entire Cone Profile
Left Flank of Cone
Right Flank of Cone
Right Flank Break in Slope
Left Flank Break in Slope
Linear (Left Flank of Cone)
Linear (Right Flank of Cone)
Linear (Right Flank Break in Slope)
Linear (Left Flank Break in Slope)

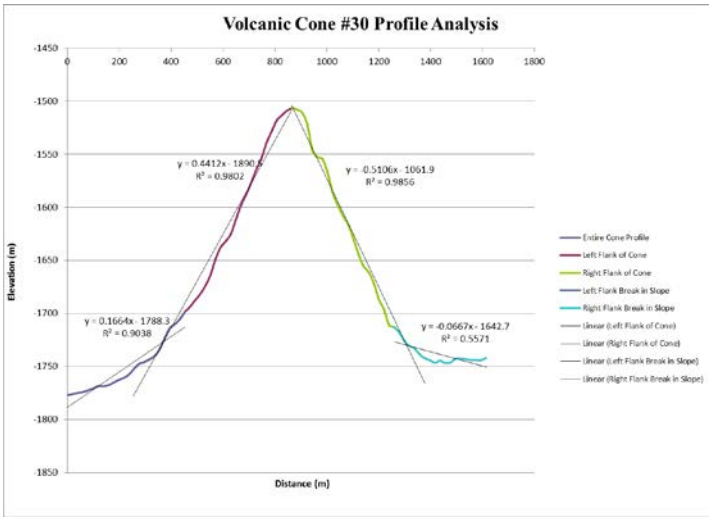
Volcanic Cone #30 Profile Analysis
Elevation (m)
Distance (m)
y = 0.4412x - 1890.5
R² = 0.9802
y = -0.5106x - 1061.9
R² = 0.9856
y = 0.1664x - 1788.3
R² = 0.9038
y = -0.0667x - 1642.7
R² = 0.5571
Entire Cone Profile
Left Flank of Cone
Right Flank of Cone
Left Flank Break in Slope
Right Flank Break in Slope
Linear (Left Flank of Cone)
Linear (Right Flank of Cone)
Linear (Left Flank Break in Slope)
Linear (Right Flank Break in Slope)

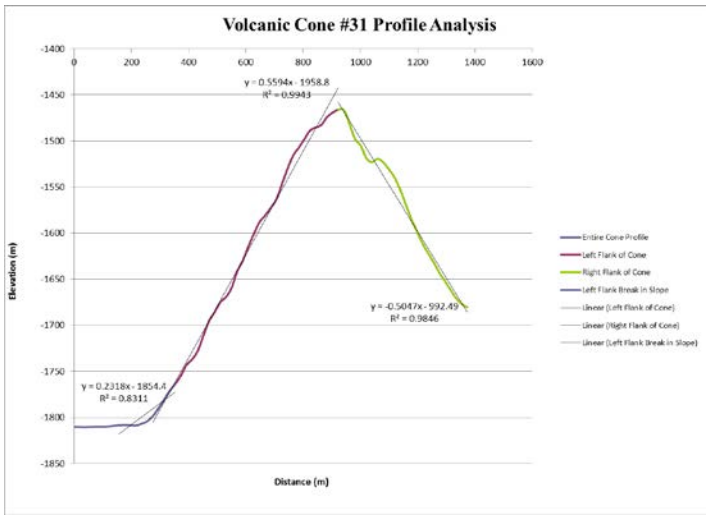
Volcanic Cone #31 Profile Analysis
y = 0.5594x - 1958.8
R² = 0.9943
y = -0.5047x - 592.49
R² = 0.9846
y = 0.2318x - 1854.4
R² = 0.8311
Elevation (m)
Distance (m)
Entire Cone Profile
Left Flank of Cone
Right Flank of Cone
Left Flank Break in Slope
Linear (Left Flank of Cone)
Linear (Right Flank of Cone)
Linear (Left Flank Break in Slope)

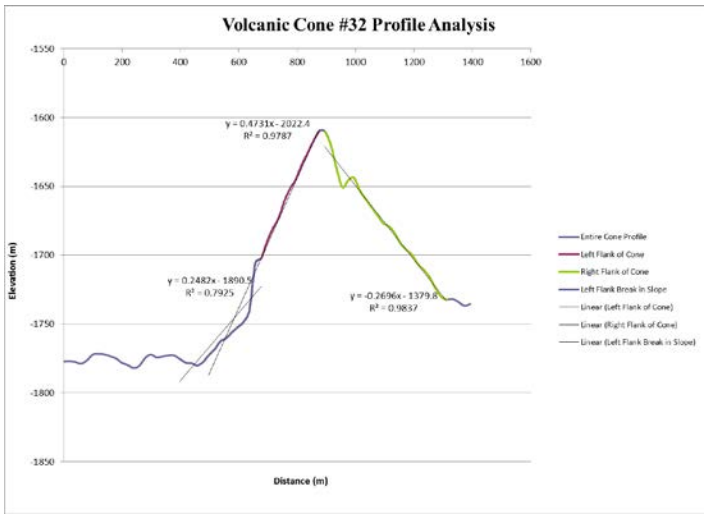
Volcanic Cone #32 Profile Analysis
y = 0.4731x - 2022.4
R² = 0.9787
y = 0.2482x - 1890.5
R² = 0.7925
y = -0.2696x - 1379.8
R² = 0.9837
Elevation (m)
Distance (m)
Entire Cone Profile
Left Flank of Cone
Right Flank of Cone
Left Flank Break in Slope
Linear (Left Flank of Cone)
Linear (Right Flank of Cone)
Linear (Left Flank Break in Slope)

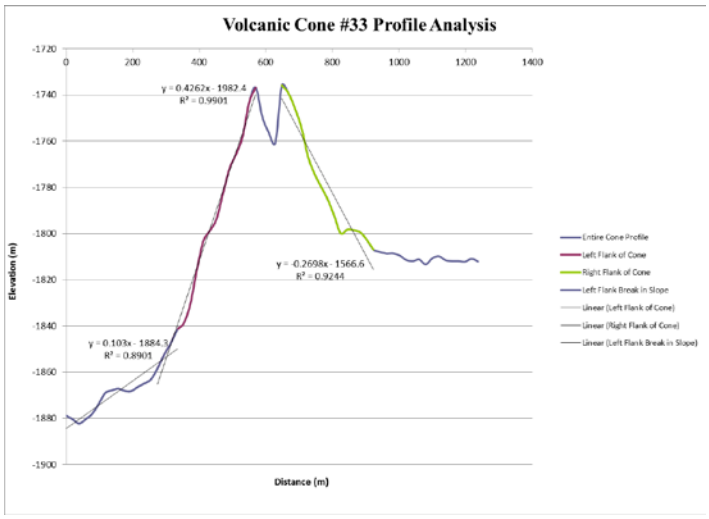
Volcanic Cone #33 Profile Analysis
y = 0.4262x - 1982.4
R² = 0.9901
y = -0.2698x - 1566.6
R² = 0.9244
y = 0.103x - 1884.3
R² = 0.8901
Elevation (m)
Distance (m)
Entire Cone Profile
Left Flank of Cone
Right Flank of Cone
Left Flank Break in Slope
Linear (Left Flank of Cone)
Linear (Right Flank of Cone)
Linear (Left Flank Break in Slope)

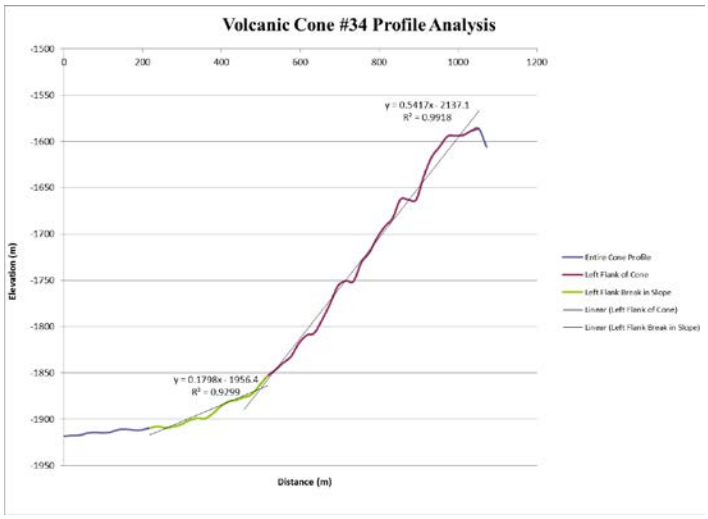
Volcanic Cone #34 Profile Analysis
y = 0.5417x - 2137.1
R² = 0.9918
y = 0.1798x - 1956.4
R² = 0.9299
Elevation (m)
Distance (m)
Entire Cone Profile
Left Flank of Cone
Left Flank Break in Slope
Linear (Left Flank of Cone)
Linear (Left Flank Break in Slope)

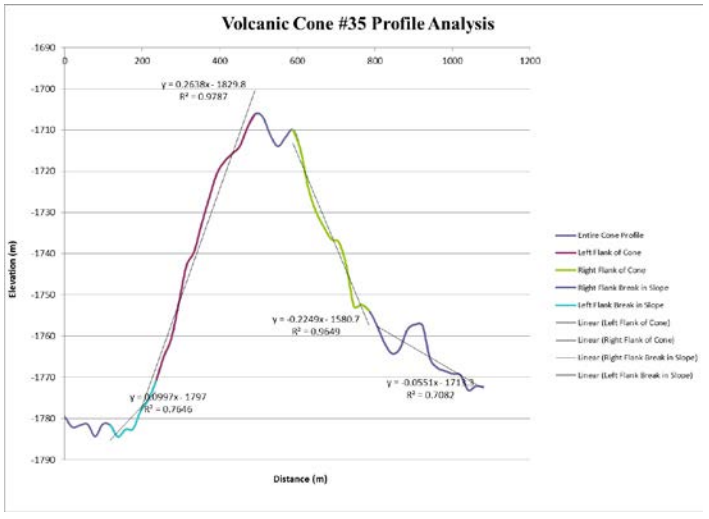
Volcanic Cone #35 Profile Analysis
y = 0.2618x - 1829.8
R² = 0.9787
y = -0.2249x - 1580.7
R² = 0.9649
y = 0.0997x - 1797
R² = 0.7646
y = -0.0551x - 1711.3
R² = 0.7082
Elevation (m)
Distance (m)
Entire Cone Profile
Left Flank of Cone
Right Flank of Cone
Right Flank Break in Slope
Left Flank Break in Slope
Linear (Left Flank of Cone)
Linear (Right Flank of Cone)
Linear (Right Flank Break in Slope)
Linear (Left Flank Break in Slope)

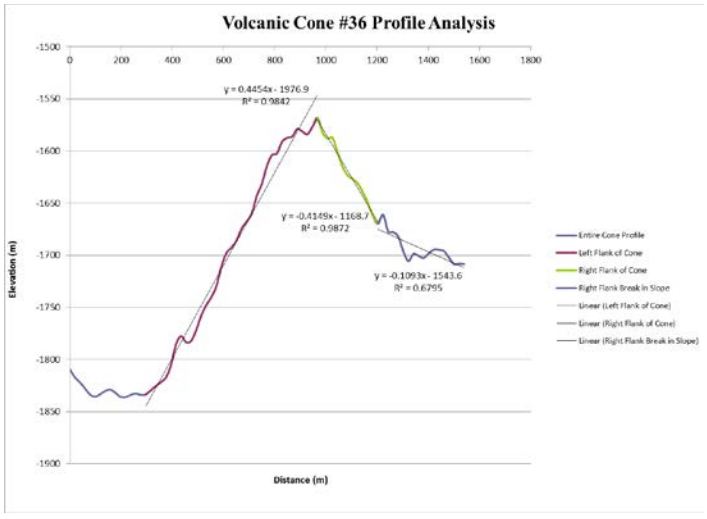
Volcanic Cone #36 Profile Analysis
y = 0.4454x - 1926.9
R² = 0.9842
y = -0.4149x - 1168.7
R² = 0.9872
y = -0.1093x - 1543.6
R² = 0.6795
Elevation (m)
Distance (m)
Entire Cone Profile
Left Flank of Cone
Right Flank of Cone
Right Flank Break in Slope
Linear (Left Flank of Cone)
Linear (Right Flank of Cone)
Linear (Right Flank Break in Slope)

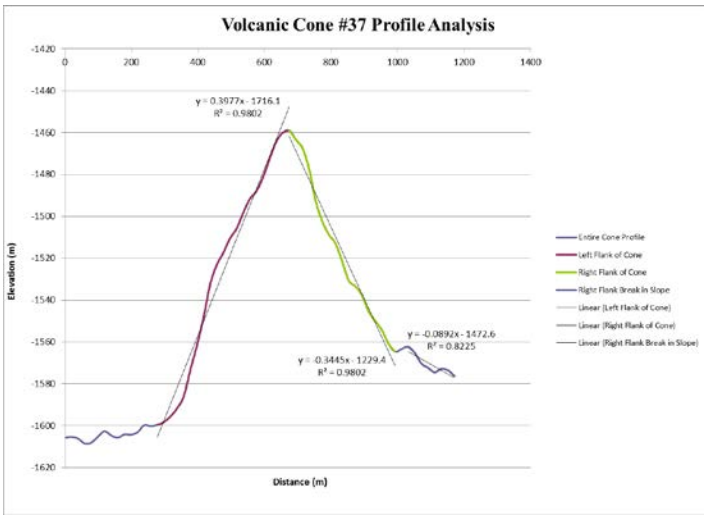
Volcanic Cone #37 Profile Analysis
y = 0.3977x - 1716.1
R² = 0.9802
y = -0.0892x - 1472.6
R² = 0.8225
y = -0.3445x - 1229.4
R² = 0.9802
Elevation (m)
Distance (m)
Entire Cone Profile
Left Flank of Cone
Right Flank of Cone
Right Flank Break in Slope
Linear (Left Flank of Cone)
Linear (Right Flank of Cone)
Linear (Right Flank Break in Slope)

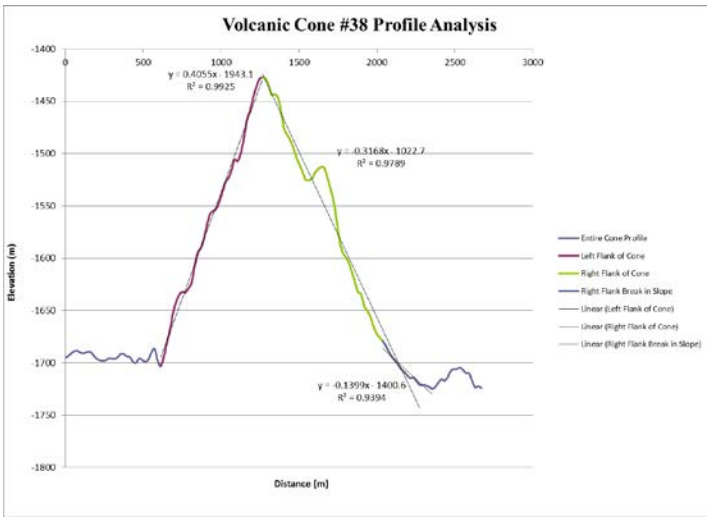
Volcanic Cone #38 Profile Analysis
y = 0.4055x - 1943.1
R² = 0.9925
y = -0.3168x - 1022.7
R² = 0.9789
y = -0.1899x - 1400.6
R² = 0.9394
Elevation (m)
Distance (m)
Entire Cone Profile
Left Flank of Cone
Right Flank of Cone
Right Flank Break in Slope
Linear (Left Flank of Cone)
Linear (Right Flank of Cone)
Linear (Right Flank Break in Slope)

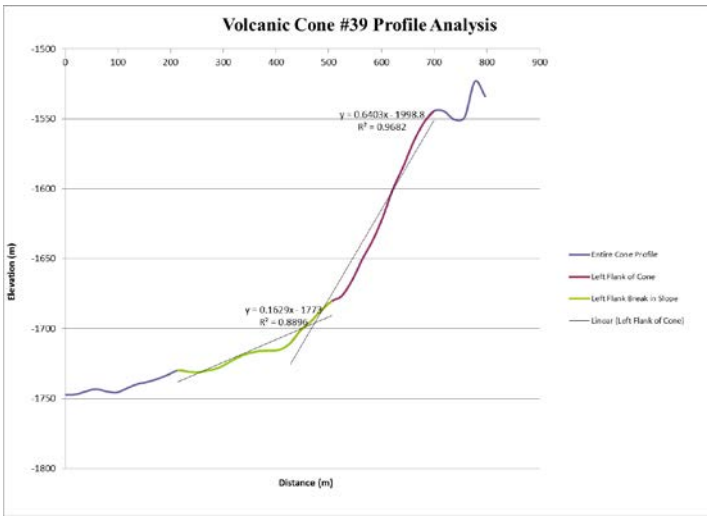
Volcanic Cone #39 Profile Analysis
y = 0.6403x - 1998.8
R² = 0.9682
y = 0.1629x - 1773
R² = 0.8896
Elevation (m)
Distance (m)
Entire Cone Profile
Left Flank of Cone
Left Flank Break in Slope
Linear (Left Flank of Cone)

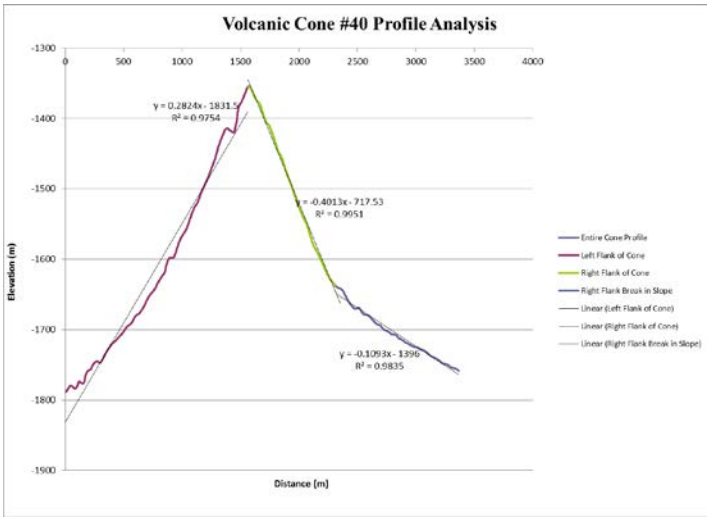
Volcanic Cone #40 Profile Analysis
y = 0.2824x - 1831.5
R² = 0.9754
y = -0.4013x - 717.53
R² = 0.9951
y = -0.1093x - 1396
R² = 0.9835
Elevation (m)
Distance (m)
Entire Cone Profile
Left Flank of Cone
Right Flank of Cone
Right Flank Break in Slope
Linear (Left Flank of Cone)
Linear (Right Flank of Cone)
Linear (Right Flank Break in Slope)

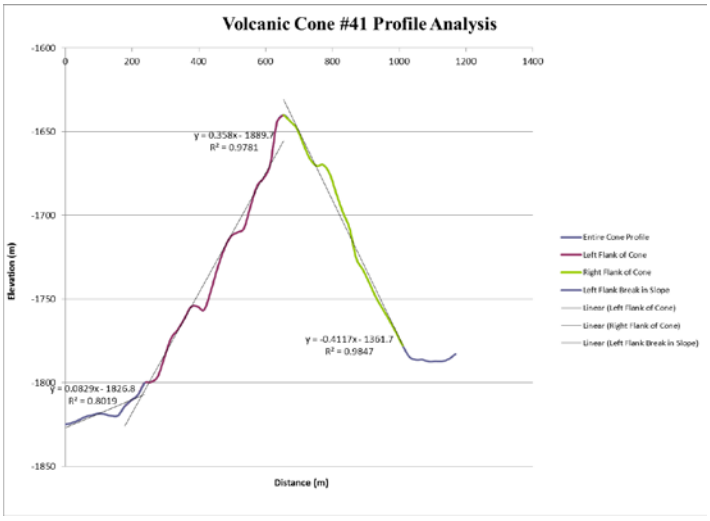
Volcanic Cone #41 Profile Analysis
y = 0.358x - 1889.7
R² = 0.9781
y = -0.4117x - 1361.7
R² = 0.9847
y = 0.0829x - 1826.8
R² = 0.8019
Elevation (m)
Distance (m)
Entire Cone Profile
Left Flank of Cone
Right Flank of Cone
Left Flank Break in Slope
Linear (Left Flank of Cone)
Linear (Right Flank of Cone)
Linear (Left Flank Break in Slope)

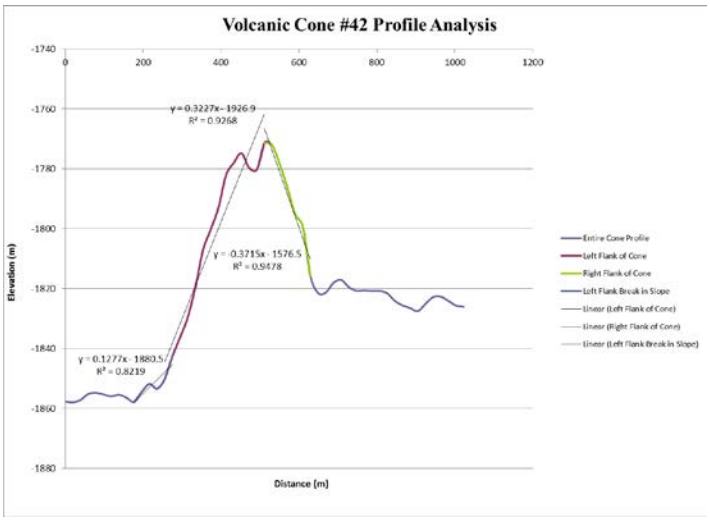
Volcanic Cone #42 Profile Analysis
y = 0.3227x - 1926.9
R² = 0.9268
y = -0.3715x - 1576.5
R² = 0.9478
y = 0.1277x - 1880.5
R² = 0.8219
Elevation (m)
Distance (m)
Entire Cone Profile
Left Flank of Cone
Right Flank of Cone
Left Flank Break in Slope
Linear (Left Flank of Cone)
Linear (Right Flank of Cone)
Linear (Left Flank Break in Slope)

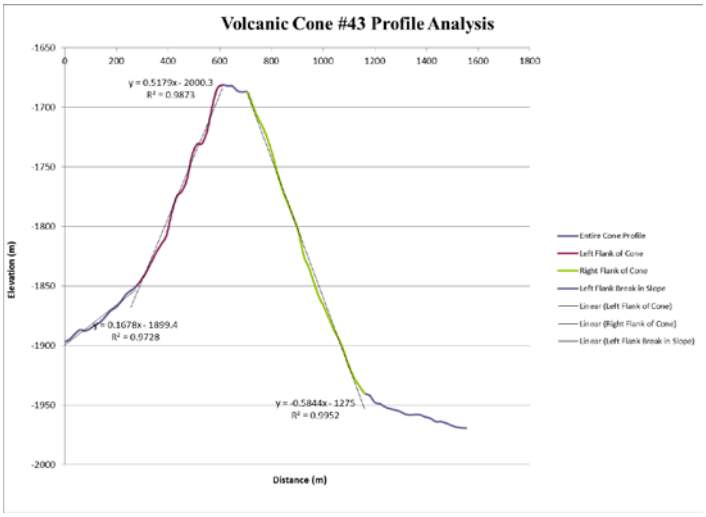
Volcanic Cone #43 Profile Analysis
y = 0.5179x - 2000.3
R² = 0.9873
y = 0.1678x - 1899.4
R² = 0.9728
y = -0.5844x - 1275
R² = 0.9952
Elevation (m)
Distance (m)
Entire Cone Profile
Left Flank of Cone
Right Flank of Cone
Left Flank Break in Slope
Linear (Left Flank of Cone)
Linear (Right Flank of Cone)
Linear (Left Flank Break in Slope)

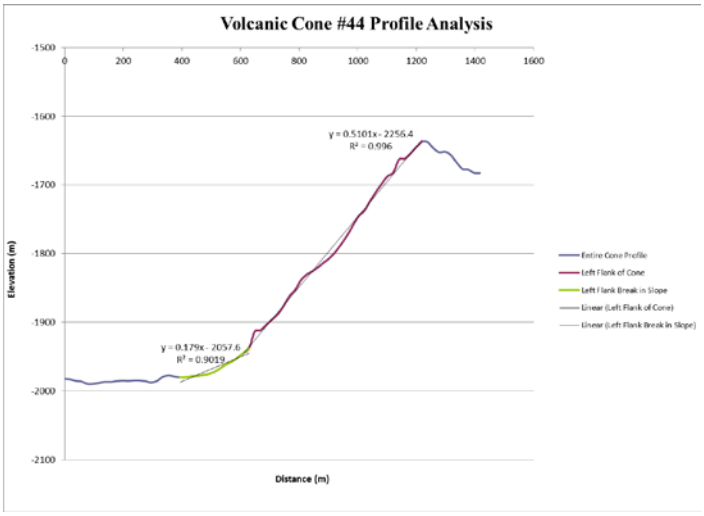
Volcanic Cone #44 Profile Analysis
y = 0.5101x - 2256.4
R² = 0.996
y = 0.179x - 2057.6
R² = 0.9019
Elevation (m)
Distance (m)
Entire Cone Profile
Left Flank of Cone
Left Flank Break in Slope
Linear (Left Flank of Cone)
Linear (Left Flank Break in Slope)

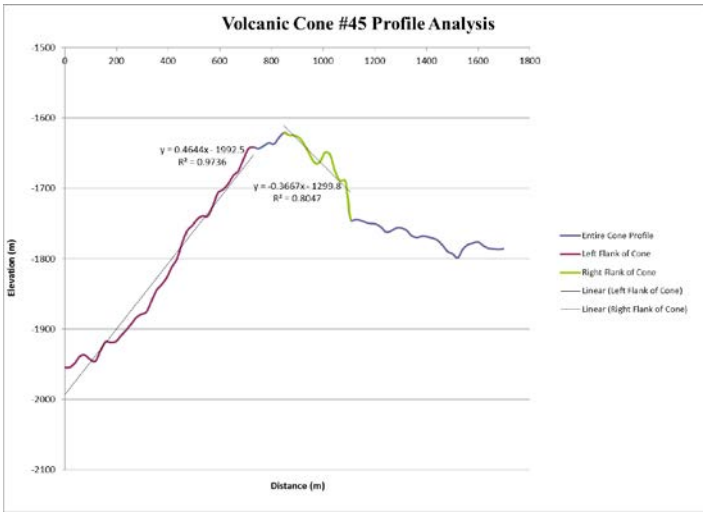
Volcanic Cone #45 Profile Analysis
y = 0.4644x - 1992.5
R² = 0.9736
y = -0.3667x - 1299.8
R² = 0.8047
Elevation (m)
Distance (m)
Entire Cone Profile
Left Flank of Cone
Right Flank of Cone
Linear (Left Flank of Cone)
Linear (Right Flank of Cone)

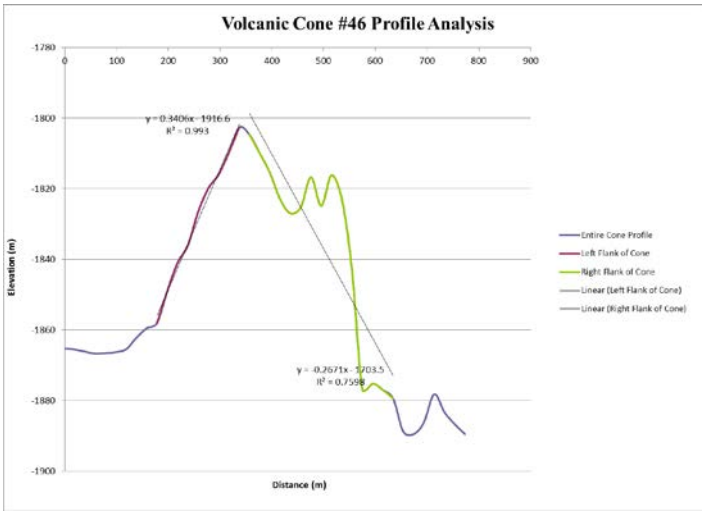
Volcanic Cone #46 Profile Analysis
y = 0.3406x - 1916.6
R² = 0.993
y = -0.2671x - 1703.5
R² = 0.7598
Elevation (m)
Distance (m)
Entire Cone Profile
Left Flank of Cone
Right Flank of Cone
Linear (Left Flank of Cone)
Linear (Right Flank of Cone)

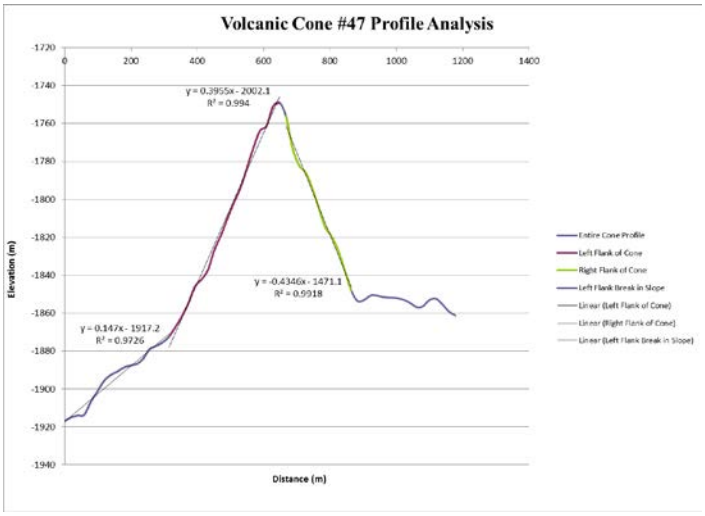
Volcanic Cone #47 Profile Analysis
y = 0.3955x - 2002.1
R² = 0.994
y = 0.147x - 1917.2
R² = 0.9726
y = -0.4346x - 1471.1
R² = 0.9918
Elevation (m)
Distance (m)
Entire Cone Profile
Left Flank of Cone
Right Flank of Cone
Left Flank Break in Slope
Linear (Left Flank of Cone)
Linear (Right Flank of Cone)
Linear (Left Flank Break in Slope)